



# Carbon export and transfer to depth across the Southern Ocean Great Calcite Belt

S. Z. Rosengard<sup>1,2</sup>, P. J. Lam<sup>1,3</sup>, W. M. Balch<sup>4</sup>, M. E. Auro<sup>1</sup>, S. Pike<sup>1</sup>, D. Drapeau<sup>4</sup>, and B. Bowler<sup>4</sup>

<sup>1</sup>Woods Hole Oceanographic Institution, Woods Hole, MA, USA

<sup>2</sup>Massachusetts Institute of Technology, Cambridge, MA, USA

<sup>3</sup>University of California, Santa Cruz, CA, USA

<sup>4</sup>Bigelow Laboratory for Ocean Sciences, Boothbay Harbor, ME, USA

Correspondence to: S. Z. Rosengard (srosengard@whoi.edu); P. J. Lam (pjlam@ucsc.edu)

Received: 29 December 2014 – Published in Biogeosciences Discuss.: 10 February 2015

Revised: 27 May 2015 – Accepted: 08 June 2015 – Published: 02 July 2015

**Abstract.** Sequestration of carbon by the marine biological pump depends on the processes that alter, remineralize, and preserve particulate organic carbon (POC) during transit to the deep ocean. Here, we present data collected from the Great Calcite Belt, a calcite-rich band across the Southern Ocean surface, to compare the transformation of POC in the euphotic and mesopelagic zones of the water column. The <sup>234</sup>Th-derived export fluxes and size-fractionated concentrations of POC, particulate inorganic carbon (PIC), and biogenic silica (BSi) were measured from the upper 1000 m of 27 stations across the Atlantic and Indian sectors of the Great Calcite Belt. POC export out of the euphotic zone was correlated with BSi export. PIC export was not, but did correlate positively with POC flux transfer efficiency. Moreover, regions of high BSi concentrations, which corresponded to regions with proportionally larger particles, exhibited higher attenuation of > 51 μm POC concentrations in the mesopelagic zone. The interplay among POC size partitioning, mineral composition, and POC attenuation suggests a more fundamental driver of POC transfer through both depth regimes in the Great Calcite Belt. In particular, we argue that diatom-rich communities produce large and labile POC aggregates, which not only generate high export fluxes but also drive more remineralization in the mesopelagic zone. We observe the opposite in communities with smaller calcifying phytoplankton, such as coccolithophores. We hypothesize that these differences are influenced by inherent differences in the lability of POC exported by different phytoplankton communities.

## 1 Introduction

The biological pump sequesters atmospheric carbon dioxide (CO<sub>2</sub>) in the ocean (Volk and Hoffert, 1985) by way of phytoplankton-driven CO<sub>2</sub> fixation, followed by the sinking of this fixed particulate organic carbon (POC) as aggregates and fecal pellets down the water column (Riley et al., 2012). The quantity per unit area and time of POC exiting the base of the euphotic zone defines the export flux, while export efficiency represents the fraction of bulk primary production comprising this flux (Buesseler, 1998). In the mesopelagic zone (from the base of the euphotic zone to ~ 1000 m), export flux attenuates due to remineralization mediated by zooplankton grazing and bacteria (Buesseler and Boyd, 2009; Giering et al., 2014; Martin et al., 1987). The flux of this processed organic carbon leaving the mesopelagic zone, only ≤ 10 % of export flux, directly scales with the quantity of atmospheric CO<sub>2</sub> sequestered by the marine biological pump over hundreds to thousands of years (Kwon et al., 2009).

On average, only ~ 1 % of the organic matter produced by phytoplankton in the surface reaches the deep sea (Martin et al., 1987). However, export and sequestration flux vary widely by region, as do export efficiencies and attenuation of export flux (Buesseler and Boyd, 2009; Buesseler et al., 2007; Henson et al., 2011, 2012b; Martin et al., 1987; Thomalla et al., 2008). Such variations may drive observed differences in the weight percent of organic carbon deposited at the sediment surface (Hedges and Oades, 1997), suggesting that the overall strength of the biological pump as a carbon sink is not globally uniform. These geographical differences have spurred decades of research into how mechanisms

in the shallower ocean – the euphotic and mesopelagic zones – alter sinking particulate organic matter during vertical transit.

As an example, Armstrong et al. (2002), Klaas and Archer (2002) and Francois et al. (2002) posited that mineral associations with sinking organic carbon could explain these variations. Their ballast hypothesis model suggested that minerals enhanced the biological pump (1) by increasing the density and, consequently, the sinking speed of particulate organic matter and (2) by inhibiting organic carbon remineralization down the water column. Expediting vertical transit decreases the time for remineralization to act on sinking particulate organic matter, increasing its chances of reaching the deep sea. The authors observed that calcite flux in the bathypelagic zone (> 1000 m) explains roughly half of the variation in the magnitude of POC flux reaching the deep sea (Klaas and Archer, 2002), and may also account for some of the observed geographical variation in POC flux attenuation with depth (Francois et al., 2002).

In its conception and infancy, the ballast hypothesis was based upon observed correlations between mineral and organic carbon fluxes in the deep (> 1000 m) sea. Yet, evidence for the ballast mechanism in the euphotic and mesopelagic zones remains equivocal, as deeper correlations are scarcely matched by shallower ocean observations (Le Moigne et al., 2012). Several surface regions do not exhibit ballast correlations between mineral flux and POC flux (e.g., Thomalla et al., 2008; Henson et al., 2012b). In the Atlantic and Southern oceans, Le Moigne et al. (2012) found a significant fraction of POC export flux to remain unassociated with minerals altogether. Moreover, tank incubations simulating POC and mineral suspensions yield conflicting results: some have observed mineral associations to increase aggregate sinking rates (Engel et al., 2009), while others find no such effect (Passow and De la Rocha, 2006). De La Rocha et al. (2008) even suggest that sticky polymers from POC might ballast sinking minerals, rather than vice versa.

The scarcity of evidence supporting a shallow ocean ballast mechanism suggests that the transit of particulate organic carbon in the surface, mesopelagic and deeper ocean is mechanistically decoupled (Lam et al., 2011; Lomas et al., 2010). Indeed, the debate surrounding the ballast hypothesis arises from a deeper issue of whether the mechanisms that influence carbon export from the euphotic zone are the same as those that control its remineralization in the mesopelagic zone, and/or its transfer beyond the mesopelagic zone into the deep sea.

The following report compares the export of organic carbon from the euphotic zone with its transfer through the mesopelagic zone across the region of the Great Calcite Belt (Balch et al., 2011a, 2014; Fig. 1). Spanning across the Southern Ocean, particularly between the subtropical and polar fronts, the Great Calcite Belt defines a highly reflective band observed from space during each austral spring and summer. Its high reflectivity is caused by calcite-rich surface

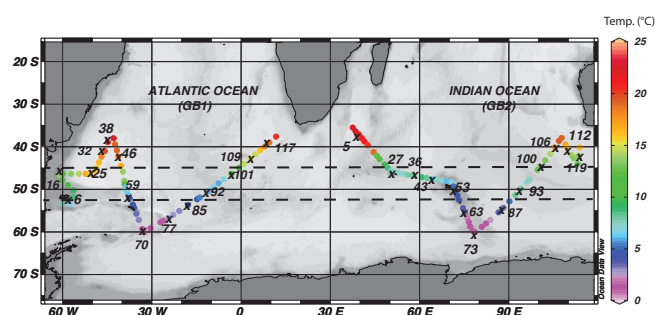


**Figure 1.** Cruise tracks across the Atlantic (cruise GB1) and Indian (cruise GB2) sectors of the Great Calcite Belt showing sea surface temperature along the two transects. Station numbers where  $^{234}\text{Th}$  and size-fractionated particles were sampled are indicated by crosses. The two horizontal dashed lines at 45 and 52° S represent the approximate locations of the Subantarctic and polar fronts, respectively (Belkin and Gordon, 1996; Sokolov and Rintoul, 2009).

waters produced by coccolithophore blooms in the Southern Ocean. In this zone, coccolithophores are more abundant than in regions north and south of the Great Calcite Belt. South of the polar front, coccolithophore abundances decline dramatically as dissolved silica concentrations increase and diatoms flourish (Balch et al., 2011a).

Spanning a large range in surface mineral concentrations, primary productivity, and phytoplankton community composition (Balch et al., 2011a), the Great Calcite Belt provides an excellent opportunity to assess the processes controlling organic carbon export, export efficiency, and attenuation of POC concentration ([POC]) with depth. Here, we report estimates of  $^{234}\text{Th}$ -derived POC fluxes and [POC] through both the euphotic and mesopelagic zones within the Atlantic and Indian sectors of the Great Calcite Belt. We focus on the upper 1000 m of the Great Calcite Belt because the attenuation of POC flux and concentration is most dramatic within this depth interval (Martin et al., 1987; Lam et al., 2011). As the following discussion illuminates, this study additionally weighs the ballast hypothesis against other mechanisms hypothesized to control the transfer of organic carbon through the water column, and ultimately into the deep sea, where carbon residence time modulates atmospheric  $p\text{CO}_2$  and climate over hundreds to thousands of years (Kwon et al., 2009).

## 2 Methods

### 2.1 Field site

Samples from the Great Calcite Belt were collected during two research cruises, GB1 and GB2, which transited the Atlantic and Indian sectors of the Great Calcite Belt during the austral summer of 2011 and 2012, respectively (Fig. 1), concurrent with the putative coccolithophore bloom (Balch et al.,

2011a). In 2011, for cruise GB1 (MV1101), the R/V *Melville* crossed the Atlantic sector from Punta Arenas, Chile, to Cape Town, South Africa, sampling between 39 and 59° S. One year later, for cruise GB2 (RR1202), the R/V *Revelle* crossed the Indian sector from Durban, South Africa, to Perth, Australia, sampling between 37 and 60° S (Table 1). Both cruise tracks crossed the subtropical, Subantarctic and polar fronts, which are approximately located at 40, 45 and 52° S (e.g., Belkin and Gordon, 1996; Sokolov and Rintoul, 2009), respectively, defining observed shifts in temperature and nutrient characteristics of the surface ocean.

Each day during GB1 and GB2, 30 L Niskin samples were collected pre-dawn for measuring primary production. A Biospherical Instruments (San Diego, CA) sensor was mounted on the CTD/rosette and referenced to a deck sensor mounted on the ship's superstructure to measure photosynthetically available radiation (PAR) during the casts. Water was then sampled at fixed light depths relative to surface irradiance to match light levels in deck-board incubators: 36.5, 21.1, 11.7, 3.55, 1.93 and 0.28 %. The light depths were calculated two ways: (a) between 10:00 and 14:00 LT (during daylight hours), percentages of surface irradiance were derived directly from the downcast PAR profile immediately preceding bottle firing, or (b) at all other times, the light levels were back-calculated from the previously determined relationship between beam transmittance and diffuse attenuation of PAR (Balch et al., 2011b). From these casts, primary production rates were measured using the  $^{14}\text{C}$  microdiffusion technique (Paasche and Brubak, 1994) with modifications by Balch et al. (2000; see also Fabry and Balch, 2010).

### 2.1.1 Size-fractionated particle collection

We report measurements of total and particulate  $^{234}\text{Th}$  activity and size-fractionated particle composition from 27 stations (Fig. 1; Table 1).

Size-fractionated particles were collected at eight depths in the upper 1000 m of 14 stations from GB1 and 13 stations from GB2, using modified battery operated in situ pumps (McLane WTS-LV). The modified pumps directed seawater through two flow paths (Lam et al., 2014), each of which passed through a "mini-MULVFS" filter holder designed to retain large particles (Bishop et al., 2012). Seawater first passed through 51  $\mu\text{m}$  polyester pre-filters in both filter holders for collection of large (> 51  $\mu\text{m}$ ) size-fraction particles, and then through paired 0.8  $\mu\text{m}$  polyethersulfone (Supor<sup>TM</sup>) filters in one flow path and paired 1  $\mu\text{m}$  quartz fiber (Whatman<sup>TM</sup> QMA) filters in the other flow path, both of which collected small (< 51  $\mu\text{m}$ ) size-fraction particles. An average of 200 and 500 L of seawater passed through the Supor and QMA flow paths over 1–2.5 h, respectively. Immediately after collection, between half and all of the > 51  $\mu\text{m}$  size-fraction particles from one flow path were rinsed off of the polyester pre-filters and onto 25 mm 1  $\mu\text{m}$  Sterlitech silver filters using 0.2  $\mu\text{m}$  filtered seawater, and dried at 50 °C

for subsequent analysis of particulate  $^{234}\text{Th}$ , particulate organic carbon (POC), and particulate inorganic carbon (PIC, or calcium carbonate). Subsamples of QMA filters were likewise dried at 50 °C for  $^{234}\text{Th}$  and POC analysis in the < 51  $\mu\text{m}$  size fraction. Finally, the polyester pre-filters from the other flow path and Supor filters were dried in a laminar flow hood at room temperature.

In the euphotic zone, where most POC is produced, these operationally defined size fractions allude primarily to the structure of phytoplankton communities producing POC (e.g., large diatoms would be found in > 51  $\mu\text{m}$  size-fraction particles). In the mesopelagic zone, which extends from the base of the euphotic zone to 1000 m in depth, > 51  $\mu\text{m}$  POC is predominantly comprised of phytoplankton and bacterial biomass that has been repackaged into aggregates and fecal pellets. The > 51  $\mu\text{m}$  particles collected at station GB1-85 illustrate these different size-fraction interpretations by depth. Shallower particles collected at 25 and 73 m, the base of the euphotic zone, are mainly comprised of intact phytoplankton cells (Fig. 2a, b). By contrast, deeper particles collected at 173 m exhibit the features of particulate aggregates and fecal pellets (Fig. 2c).

## 2.2 Particle composition

Bulk concentrations of POC, PIC, biogenic silica (BSi), and particulate  $^{234}\text{Th}$  activity were measured in both < 51 and > 51  $\mu\text{m}$  fractions of particles collected at each station. POC concentrations were measured at all depths of the profiles, while [PIC] and [BSi] were mainly measured at select depths above 200 m and at the deepest depth (800–1000 m) of the profile. Particulate  $^{234}\text{Th}$  activities in all subfractions of > 51  $\mu\text{m}$  (25 mm silver filters) and < 51 (25 mm QMA filters) samples were measured using low-level Risø beta counters immediately on the ship and in the lab at least six  $^{234}\text{Th}$  half-lives post-collection for background activity.

After counting for  $^{234}\text{Th}$  background activity, ~ 25 % of the silver filter (~ 115 L equivalent) was fumed overnight (12–17 h) with concentrated hydrochloric acid to remove inorganic carbon, before measuring > 51  $\mu\text{m}$  [POC] using an elemental CHN analyzer. A similar protocol was followed to measure < 51  $\mu\text{m}$  [POC] from one 12 mm diameter subsample of each QMA filter, representing ~ 1 % of the entire sample (~ 5 L equivalent). Vertical profiles of > 51 and < 51  $\mu\text{m}$  [POC] between the base of the euphotic zone and the deepest measurement at 800–1000 m were fitted to a power-law function to describe the attenuation of [POC] with depth, based on a function first applied to POC flux by Martin et al. (1987) and then analogously to POC concentration by Lam and Bishop (2007),

$$[\text{POC}]_z = [\text{POC}]_0 \left( \frac{z}{z_{\text{PAR}}} \right)^{-b}, \quad (1)$$

where, at most stations,  $z_{\text{PAR}}$  represents the depth of 0.3 % PAR (see Sect. 2.4). The exponent  $b$  represents the attenu-

**Table 1.** Locations and times of sampling of total  $^{234}\text{Th}$  and size-fractionated particles on cruises GB1 and GB2. Two export depths are indicated:  $z_{\text{PAR}}$  (depth of 0.3 % of surface photosynthetically available radiation) and  $z_{\text{Th/U}}$  (depth where  $^{234}\text{Th}$  and  $^{238}\text{U}$  activities return to secular equilibrium below surface deficits).

Cruise	Station	Date	Lat.	Long.	$z_{\text{PAR}}$	$z_{\text{Th/U}}$
–	–	dd/mm/yy	° N	° E	m	m
GB1	6	14 Jan 2011	−51.79	−56.11	79	130
GB1	16	17 Jan 2011	−46.26	−59.83	62	141
GB1	25	20 Jan 2011	−45.67	−48.95	62	115
GB1	32	22 Jan 2011	−40.95	−46.00	69	171
GB1	38	24 Jan 2011	−36.52	−43.38	121	121
GB1	46	26 Jan 2011	−42.21	−41.21	63	100
GB1	59	29 Jan 2011	−51.36	−37.85	60	95
GB1	70	1 Feb 2011	−59.25	−33.15	100	100
GB1	77	3 Feb 2011	−57.28	−25.98	98	100
GB1	85	5 Feb 2011	−53.65	−17.75	73	140
GB1	92	7 Feb 2011	−50.40	−10.80	59	100
GB1	101	9 Feb 2011	−46.31	−3.21	81	140
GB1	109	11 Feb 2011	−42.63	3.34	76	130
GB1	117	13 Feb 2011	−38.97	9.49	62	110
GB2	5	21 Feb 2012	−36.94	39.60	78	90
GB2	27	26 Feb 2012	−45.82	51.05	105	105
GB2	36	28 Feb 2012	−46.84	58.25	90	90
GB2	43	1 Mar 2012	−47.53	64.01	108	125
GB2	53	3 Mar 2012	−49.30	71.32	81	100
GB2	63	5 Mar 2012	−54.40	74.54	109	130
GB2	73	7 Mar 2012	−59.71	77.73	93	75
GB2	87	10 Mar 2012	−54.23	88.22	107	100
GB2	93	11 Mar 2012	−49.81	94.13	113	130
GB2	100	14 Mar 2012	−44.62	100.50	113	90
GB2	106	16 Mar 2012	−40.10	105.34	102	95
GB2	112	17 Mar 2012	−40.26	109.63	76	105
GB2	119	20 Mar 2012	−42.08	113.40	92	90

ation coefficient, with higher attenuation coefficients (more negative exponents) for profiles with greater attenuation of  $> 51 \mu\text{m}$  [POC] with depth. We focus our discussion on the attenuation of  $> 51 \mu\text{m}$  [POC], because we assume that they contribute disproportionately to sinking fluxes compared to the  $< 51 \mu\text{m}$  size fraction (McCave, 1975; Lam and Bishop, 2007; Lam et al., 2011). Figure 3 and Table 2 show all significant ( $p < 0.05$ ) power-law fits for  $> 51 \mu\text{m}$  [POC] profiles.

PIC in the samples was assumed to be biomineral calcium carbonate ( $\text{CaCO}_3$ ), and was derived from particulate calcium (Ca) corrected for salt Ca using a seawater 0.0382 Ca : Na ( $g : g$ ) ratio (Lam and Bishop, 2007; Pilson, 2012). In the in situ pump samples, salt-derived Ca typically accounted for  $\sim 60\%$  of total Ca. The  $> 51 \mu\text{m}$  PIC size-fraction concentrations were measured mainly in subsamples of remaining pre-filter material and occasionally in subfractions of the silver filters, if the former were unavailable. The  $< 51 \mu\text{m}$  size-fraction [PIC] was measured in three 12mm circular QMA subsamples, representing  $\sim 15 \text{L}$  or  $\sim 3\%$  of the sample. Subsamples were leached in 0.6 N ultrapure Seastar™ Baseline hydrochloric acid (HCl) at  $60^\circ\text{C}$  for 12–16 h. The

leachate was subsequently filtered through a  $0.4 \mu\text{m}$  polycarbonate membrane filter, diluted to 0.12 N HCl, and spiked with 1 ppb of indium as an internal standard. The spiked leachate solution was then analyzed for Ca, Na and P using an Element 2 sector-field inductively coupled plasma mass spectrometer (ICP-MS) at medium and high resolution. Counts per second were converted to concentration using external mixed element standard curves.

For measuring  $> 51$  and  $< 51 \mu\text{m}$  [BSi], prefilter or Supor subsamples, respectively, were leached in 0.2 N sodium hydroxide at  $85^\circ\text{C}$  for 1 h and then analyzed by standard spectrophotometric detection of the blue silico-molybdate complex in each leachate within 24 h of the leach (Strickland and Parsons, 1968; Brzezinski and Nelson, 1989). Absorbance through each sample was converted to concentration using an external Si standard curve.

### 2.3 $^{234}\text{Th}$ -derived flux estimates

Particle fluxes were estimated at each station by measuring the water-column disequilibrium between  $^{234}\text{Th}$  and  $^{238}\text{U}$  in the upper 350 m of the water column (Savoie et al., 2006).

**Table 2.** POC fluxes, concentrations, and attenuation of  $> 51 \mu\text{m}$  [POC] in the mesopelagic zone. Attenuation coefficient is the exponent from significant power-law fits to  $> 51 \mu\text{m}$  [POC].  $z_{\text{PAR}}+100\text{m}$  is 100 m below  $z_{\text{PAR}}$ , as defined in the Table 1 caption. Transfer efficiency is POC flux at  $z_{\text{PAR}}+100\text{m}$  divided by POC flux at  $z_{\text{PAR}}$ . Deep  $> 51 \mu\text{m}$  [POC] was measured at 1000 m and 800 m for GB1 and GB2, respectively. POC flux errors are propagated from  $^{234}\text{Th}$  flux and POC:  $^{234}\text{Th}$  errors.

Cruise	Station	Depth	$> 51 \mu\text{m}$ [POC]	Attenuation coefficient	$^{234}\text{Th}$ flux at $z_{\text{PAR}}+100\text{m}$	POC:Th at $z_{\text{PAR}}+100\text{m}$	POC flux at $z_{\text{PAR}}+100\text{m}$	Transfer efficiency	$> 51 \mu\text{m}$ [POC] ( $\geq 800\text{m}$ )
–	–	m		unitless	$\text{dpm m}^{-2} \text{d}^{-1}$	$\mu\text{mol dpm}^{-1}$	$\text{mmol m}^{-2} \text{d}^{-1}$	unitless	$\mu\text{M}$
GB1	6	179		0.8	$3319 \pm 128^c$	1.7	$5.7 \pm 0.31$	1.00	0.030
GB1	16	162		1.1	$2567 \pm 116^c$	2.4	$6.1 \pm 0.30$	1.04	No data
GB1	25	162		0.4	$1074 \pm 125$	2.5	$2.7 \pm 0.37$	1.76	0.013
GB1	32	169		0.9	$1581 \pm 186$	1.3	$2.0 \pm 0.25$	0.86	0.006
GB1	38	221		No fit	$911 \pm 206$	1.6	$1.5 \pm 0.35$	0.70	0.026
GB1	46	163		1.0	$1937 \pm 146$	1.6	$3.1 \pm 0.27$	0.4	0.009
GB1	59	160		0.6	$2582 \pm 126^c$	3.7	$9.5 \pm 0.56$	1.29	0.014
GB1	70	200		0.6	$1414 \pm 248$	3.5	$5.0 \pm 0.90$	0.90	0.024
GB1	77	198		0.5	$1903 \pm 162$	2.1	$4.0 \pm 0.41$	0.44	0.012
GB1	85	173		1.7 <sup>a</sup>	$2076 \pm 207$	3.9	$8.1 \pm 0.83$	0.41	0.035
GB1	92	159		1.1	$1339 \pm 170$	3.7	$4.9 \pm 0.64$	0.61	0.019
GB1	101	181		0.8	$1774 \pm 135$	1.7	$3.0 \pm 0.24$	0.83	0.019
GB1	109	176		1.0	$1719 \pm 97$	1.1	$1.9 \pm 0.13$	0.87	0.006
GB1	117	162		1.1	$1258 \pm 86$	1.2	$1.5 \pm 0.13$	0.87	0.005
GB2	5	178		0.5	$1402 \pm 3706^c$	1.1	$1.5 \pm 6.1$	0.5	No data
GB2	27	205		No fit	$2063 \pm 205$	1.2	$2.5 \pm 0.30$	0.71	No data
GB2	36	190		1.5	$1077 \pm 194$	0.9	$0.93 \pm 0.18$	0.48	0.011
GB2	43	208		1.9	$1247 \pm 200$	2.2	$2.7 \pm 0.45$	0.54	0.005
GB2	53	181		No fit	$1013 \pm 220$	2.0	$2.0 \pm 0.45$	0.49	No data
GB2	63	209		1.8	$1292 \pm 262$	1.7	$2.1 \pm 0.46$	0.31	0.014
GB2	73	193		1.5	$807 \pm 189$	1.9	$1.6 \pm 0.37$	0.48	0.008
GB2	87	207		0.7	$1213 \pm 196$	1.6	$1.9 \pm 0.34$	0.60	0.013
GB2	93	213		2.3 <sup>b</sup>	$469 \pm 249$	1.6	$0.77 \pm 0.42$	0.53	0.001
GB2	100	213		0.8	$1132 \pm 190$	0.7	$0.80 \pm 0.15$	0.52	0.014
GB2	106	202		0.9	$1405 \pm 186$	1.3	$1.8 \pm 0.26$	1.63	0.017
GB2	112	176		1.3	$270 \pm 186$	0.9	$0.23 \pm 0.21$	0.24	0.007
GB2	119	192		No fit	$756 \pm 218$	0.8	$0.57 \pm 0.17$	0.20	0.013

<sup>a</sup> Attenuation coefficient is 2.35 when only fitting  $> 51 \mu\text{m}$  [POC] measurements at depths  $< 500\text{m}$  (Fig. 3). <sup>b</sup> Outlier approximated by Chauvenet's theorem (Glover et al., 2011).

<sup>c</sup> Values were estimated by linear interpolation of values at upper and lower depths around  $z_{\text{PAR}}+100\text{m}$ . "no data": no measurements at these depths. "no fit": power-law fit was not statistically significant ( $p > 0.05$ ).

$^{234}\text{Th}$  is the radioactive daughter of  $^{238}\text{U}$  with a short enough half-life (24.1 days) relative to  $^{238}\text{U}$  such that it is assumed to be in secular equilibrium with its parent isotope in the absence of particle scavenging (i.e.,  $^{234}\text{Th}$  activity =  $^{238}\text{U}$  activity). Disequilibria between the two isotope activities in the water column are attributed to the scavenging of  $^{234}\text{Th}$  by sinking particles (Savoye et al., 2006). Integrating the deficit in  $^{234}\text{Th}$  relative to  $^{238}\text{U}$  provides a measure of particle flux down the water column (Buesseler et al., 2006). Because of the short half-life of  $^{234}\text{Th}$ , deviation from secular equilibrium exists only in regions of high particle flux. Thus,  $^{234}\text{Th}$ -based flux estimates are most frequently applied in the euphotic zone of the ocean, where particle export is maximal.

$^{234}\text{Th}$ - $^{238}\text{U}$  deficits were determined by measuring total water-column activities of both isotopes.  $^{238}\text{U}$  activity ( $A_{\text{U}-238}$ ) profiles were calculated from salinity by the following relationship (Owens et al., 2011):

$$A_{\text{U}-238} \left( \frac{\text{dpm}}{\text{L}} \right) = (0.0786 \cdot \text{Salinity}) - 0.315. \quad (2)$$

Total water-column  $^{234}\text{Th}$  activity ( $A_{\text{Th}-234}$ ) profiles were determined from 4 L seawater samples collected by CTD casts down to 300–350 m at each station (Pike et al., 2005). Shortly after collection, each 4 L seawater sample was acidified to pH 2 using concentrated nitric acid ( $\text{HNO}_3$ ), spiked with 1 g of  $^{230}\text{Th}$  of a known activity ( $50.06 \text{dpm g}^{-1}$ ) as a yield monitor, equilibrated for 8 h, and finally brought up to pH 8.5 using ammonium hydroxide ( $\text{NH}_4\text{OH}$ ; Rutgers van der Loeff et al., 2006). Manganese chloride ( $\text{MnCl}_2$ ) and potassium permanganate ( $\text{KMnO}_4$ ) were added to the neutralized seawater to form a manganese oxide ( $\text{MnO}_2$ ) precipitate, which efficiently scavenges both natural  $^{234}\text{Th}$  and added  $^{230}\text{Th}$ . After 12 h, the precipitate was filtered onto a quartz fiber filter, dried at  $50^\circ\text{C}$ , and then mounted beneath a sheet of Mylar and aluminum foil.  $^{234}\text{Th}$  activity in the precipitate was measured onboard by low-level Risø beta counters and post-cruise after at least six  $^{234}\text{Th}$  half-lives for background activity. The  $^{230}\text{Th}$  spike was recovered by fully dissolving the  $\text{MnO}_2$  precipitate, adding a 1 g spike of  $^{229}\text{Th}$  of a known activity ( $69.74 \text{dpm g}^{-1}$ ), and measuring

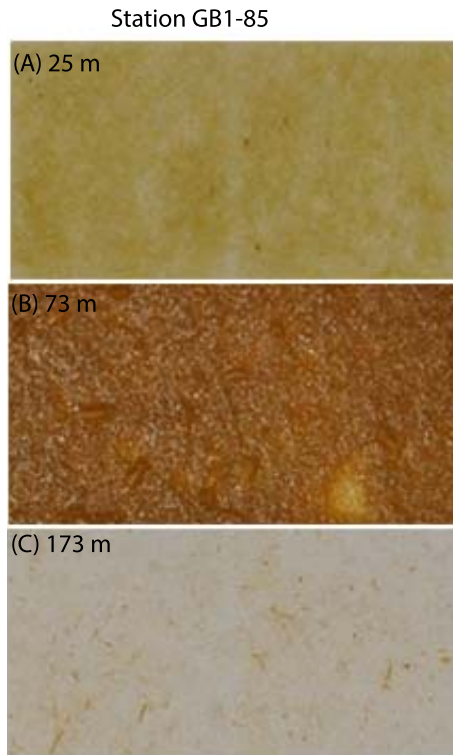


**Figure 2.** Digital images of  $> 51 \mu\text{m}$  filters from station GB1-85 (refer to Fig. 1 for station location).  $> 51 \mu\text{m}$  particles are from (a) 25 m in the euphotic zone; (b) 73 m, which corresponds to  $z_{\text{PAR}}$ , as defined in Table 1; and (c) at 173 m, below both metrics of export depth,  $z_{\text{PAR}}$  and  $z_{\text{Th/U}}$  (Table 1).  $> 51 \mu\text{m}$  particles in the euphotic zone appear as dense sheets of intact cells packed onto the filters (a, b) and as more sparsely arranged cylindrical fecal pellets on filters collected below  $z_{\text{PAR}}$  (c).

$^{229}\text{Th} : ^{230}\text{Th}$  ratios on an Element 2 sector-field ICP-MS at low resolution. Recovery of  $^{230}\text{Th}$  spike was derived from this ratio, and was used to correct for inefficiencies in the scavenging of total seawater  $^{234}\text{Th}$  by  $\text{MnO}_2$  precipitation.

To calibrate beta counting efficiency for each cruise, total deep-water (i.e., below 2000 m)  $^{234}\text{Th}$  activities were compared to total deep-water  $^{238}\text{U}$  activities, as measured in 4–5 replicate samples from two to three deep-water CTD casts during each cruise (at 5000 m during GB1, and at 2500 m during GB2). Beta counting efficiencies were adjusted such that  $^{234}\text{Th}$  and  $^{238}\text{U}$  activities were equal in these deep measurements, as secular equilibrium would be expected at such depths. We only report upper water-column activities ( $< 350$  m) after correcting for experimental efficiencies in both the seawater collection process and beta detector counting. Uncertainties in the total  $^{234}\text{Th}$  activity profiles averaged 4.5 % and were propagated from errors associated with counting statistics, recoveries, and beta-counting efficiency.

To calculate  $^{234}\text{Th}$  export flux,  $^{234}\text{Th}$  activity deficits were integrated down to the base of the euphotic zone ( $z_{\text{PAR}}$ )

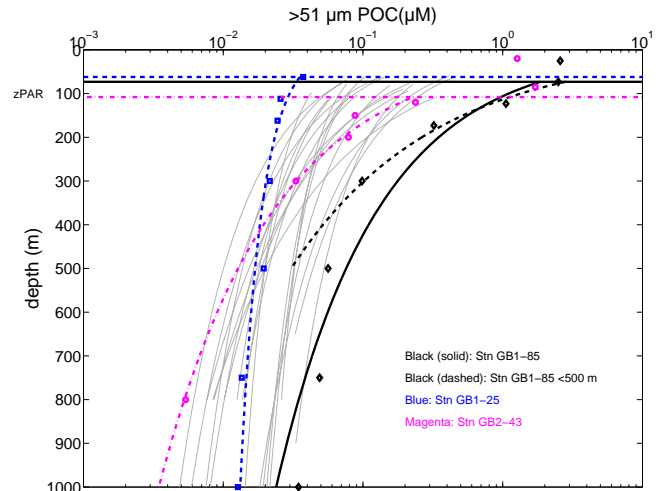


**Figure 3.** Significant power-law fits of  $> 51 \mu\text{m}$  [POC] below  $z_{\text{PAR}}$ , according to Eq. (1). Only the 22 significant fits are shown as lines. Three stations are highlighted to show the range in  $> 51 \mu\text{m}$  [POC] attenuation across GB1 and GB2 profiles (symbols represent measurements): GB1-85 had the highest POC concentration through the water column and an attenuation coefficient of 1.7; GB1-25 had the lowest attenuation coefficient (0.4); GB2-43 had the highest attenuation coefficient (1.9; Table 2). Fitting GB1-85  $> 51 \mu\text{m}$  [POC] measurements between  $z_{\text{PAR}}$  and 500 m yields a higher attenuation coefficient of 2.35. Refer to Fig. 1 for station locations.

(Buesseler et al., 2008; Thomalla et al., 2008):

$$^{234}\text{Th Flux} \left( \frac{\text{dpm}}{\text{m}^2 \text{d}} \right) = \int_0^{z_{\text{PAR}}} (A_{\text{U}-238} - A_{\text{Th}-234}) dz. \quad (3)$$

At most stations, the export depth,  $z_{\text{PAR}}$ , was chosen to be the depth where light levels were 0.3 % of surface-level PAR. The exception was station GB2-27, which did not include a PAR measurement profile. For this station, the  $z_{\text{PAR}}$  value of 105 m was defined as the depth where the transmissometry-based particle concentration decreased. These export depths were compared to one additional metric describing particle concentration in seawater: the depths where  $^{234}\text{Th}$  and  $^{238}\text{U}$  activities re-established secular equilibrium, or  $z_{\text{Th/U}}$ . We explore the sensitivity of  $^{234}\text{Th}$  flux estimates to choice of  $z_{\text{PAR}}$  in Sects. 3 and 4.1.

$^{234}\text{Th}$  flux estimates were converted to POC, PIC, and BSi fluxes by multiplication by ratios of  $> 51 \mu\text{m}$  POC, PIC, and BSi concentrations to particulate  $^{234}\text{Th}$  activity in samples at  $z_{\text{PAR}}$  (Thomalla et al., 2008; Sanders et al., 2010):

$$\text{POC Flux} \left( \frac{\mu\text{mol}}{\text{m}^2 \text{d}} \right) = [\text{POC}] : A_{\text{Th}-234} \cdot ^{234}\text{Th Flux} \left( \frac{\text{dpm}}{\text{m}^2 \text{d}} \right), \quad (4)$$

$$\text{PIC Flux} \left( \frac{\mu\text{mol}}{\text{m}^2 \text{d}} \right) = [\text{PIC}] : A_{\text{Th}-234} \cdot ^{234}\text{Th Flux} \left( \frac{\text{dpm}}{\text{m}^2 \text{d}} \right), \quad (5)$$

$$\text{Si Flux} \left( \frac{\mu\text{mol}}{\text{m}^2 \text{d}} \right) = [\text{BSi}] : A_{\text{Th}-234} \cdot ^{234}\text{Th Flux} \left( \frac{\text{dpm}}{\text{m}^2 \text{d}} \right). \quad (6)$$

## 2.4 Interpolation of data

In all cases where  $^{234}\text{Th}$  activity,  $> 51$  and  $< 51 \mu\text{m}$  [POC] and mineral concentrations, and  $> 51 \mu\text{m}$  particulate  $^{234}\text{Th}$  measurements were unavailable at  $z_{\text{PAR}}$ , linear interpolations between the sampling depths above and below  $z_{\text{PAR}}$  were used to estimate a value at the export depth (Table 1). The  $> 51$  and  $< 51 \mu\text{m}$  size-fraction POC concentrations were interpolated by the power-law attenuation function when fits were significant ( $p < 0.05$ ), or linearly when these power-law fits were not significant or inconsistent with the broader shape of the [POC] profile at that particular station. In general, corresponding POC :  $^{234}\text{Th}$ , BSi :  $^{234}\text{Th}$ , and PIC :  $^{234}\text{Th}$  ratios are quotients of these interpolated values except as noted in Tables 2 and 3.

## 3 Results

$^{234}\text{Th}$  activity profiles were measured over the upper 300–350 m at the 27 stations of cruises GB1 and GB2 (Fig. 4; Table S1 in the Supplement). Each activity profile is associated with two metrics that have been used in previous studies to define the export depth (see Sect. 2.4): the base of the euphotic zone ( $z_{\text{PAR}}$ ), which we define at 0.3 % surface PAR (e.g., Buesseler and Boyd 2009), and  $z_{\text{Th/U}}$ , where  $^{234}\text{Th}$  and  $^{238}\text{U}$  activities re-establish secular equilibrium (Table 1). In most stations, profiles exhibited  $^{234}\text{Th}$  activity deficits over a range from the surface to 75–170 m in depth, below which  $^{234}\text{Th}$  activity generally returned to secular equilibrium with  $^{238}\text{U}$  activity, within error. The notable exceptions were profiles at stations GB1-6 and GB1-16, which did not return to secular equilibrium by 170 m in depth. Considering that stations GB1-6 and GB1-16 are closest to shore, their sustained  $^{234}\text{Th}$  deficits may have been influenced by lateral advection of particles from the continental shelf. At these stations,  $z_{\text{Th/U}}$  depths were approximated by the depth below which  $^{234}\text{Th}$  activities remain constant with depth. For example, at station GB1-6,  $z_{\text{Th/U}} = 130$  m because below this depth  $^{234}\text{Th}$  activities remained relatively constant.

In the Atlantic sector, sampled in January–February 2011, all observed  $z_{\text{PAR}}$  depths were significantly shallower than  $z_{\text{Th/U}}$  depths (Student's  $t$  test  $p < 0.05$ ); on average,  $z_{\text{PAR}}$  was  $66 \pm 44$  % shallower than  $z_{\text{Th/U}}$ . By contrast, in the Indian sector, sampled roughly a year later in February–March 2012,  $z_{\text{PAR}}$  was not significantly different from  $z_{\text{Th/U}}$  ( $p > 0.05$ ), and the average relative difference was  $-6 \pm 29$  %. In general, when water-column  $^{234}\text{Th}$  activity is at steady state, the euphotic zone should correspond to the region of  $^{234}\text{Th}$  deficit relative to  $^{238}\text{U}$  (Buesseler et al., 2008; Buesseler and Boyd, 2009), i.e.,  $z_{\text{PAR}}$  should equal  $z_{\text{Th/U}}$ .

Using integrated activity deficits, export fluxes of  $^{234}\text{Th}$ , POC, PIC, and BSi at  $z_{\text{PAR}}$  were estimated at the 27 sites (Figs. 5, 6; Table 3). Overall mean  $^{234}\text{Th}$  fluxes at  $z_{\text{PAR}}$  were  $1413 \pm 432 \text{ dpm m}^{-2} \text{ d}^{-1}$  (mean  $\pm 1$  SD), and ranged from

$717 \text{ dpm m}^{-2} \text{ d}^{-1}$  at station GB2-112 to  $2437 \text{ dpm m}^{-2} \text{ d}^{-1}$  at GB1-6. Mean derived POC fluxes at  $z_{\text{PAR}}$  were  $4.5 \pm 3.9 \text{ mmol m}^{-2} \text{ d}^{-1}$ , ranging from  $0.97 \text{ mmol m}^{-2} \text{ d}^{-1}$  at station GB2-112 to  $20 \text{ mmol m}^{-2} \text{ d}^{-1}$  at GB1-85. Mean PIC fluxes were  $1.2 \pm 1.7 \text{ mmol m}^{-2} \text{ d}^{-1}$ , and ranged from  $0.067 \text{ mmol m}^{-2} \text{ d}^{-1}$  at station GB2-73 to  $6.2 \text{ mmol m}^{-2} \text{ d}^{-1}$  at GB1-59. Finally, mean BSi fluxes at  $z_{\text{PAR}}$  were  $3.8 \pm 5.8 \text{ mmol m}^{-2} \text{ d}^{-1}$ , ranging from  $0.17 \text{ mmol m}^{-2} \text{ d}^{-1}$  at station GB2-46 to  $28 \text{ mmol m}^{-2} \text{ d}^{-1}$  at GB1-85. Higher POC export stations frequently corresponded with higher BSi export stations (e.g., station GB1-85), but less so with higher PIC export stations.

The highest and lowest measured biomineral (PIC and BSi) fluxes at  $z_{\text{PAR}}$  were in GB1 and GB2, respectively, but mean values were not significantly different between ocean basins because of high variability within each basin (Fig. 6). However, mean POC fluxes at  $z_{\text{PAR}}$  were significantly higher in GB1 (mean  $\pm 1$  SD =  $6.0 \pm 4.9 \text{ mmol m}^{-2} \text{ d}^{-1}$ ) than in GB2 ( $3.0 \pm 1.7 \text{ mmol m}^{-2} \text{ d}^{-1}$ ; Student's  $t$  test  $p > 0.05$ ). Because POC :  $^{234}\text{Th}$  values did not differ between GB1 and GB2 ( $p < 0.05$ ), we attribute this inter-basin difference in POC fluxes primarily to significantly higher  $^{234}\text{Th}$  fluxes in GB1 ( $1574 \pm 463 \text{ dpm m}^{-2} \text{ d}^{-1}$ ) relative to fluxes in GB2 ( $1240 \pm 330 \text{ dpm m}^{-2} \text{ d}^{-1}$ ).

Further, there were significant latitudinal differences among export fluxes and particulate composition ratios in three temperature/nutrient regimes across both sectors (Fig. 1; Table 4): (1) north of  $45^\circ \text{S}$ , the approximate location of the Subantarctic Front, where temperatures exceeded  $\sim 10^\circ \text{C}$ ; (2) south of  $52^\circ \text{S}$ , the approximate location of the polar front (e.g., Belkin and Gordon, 1996; Sokolov and Rintoul, 2009), where temperatures remained below  $\sim 5^\circ \text{C}$ ; and (3) between  $45$  and  $52^\circ \text{S}$ , where temperatures ranged from  $\sim 5$  to  $10^\circ \text{C}$ . The  $> 51 \mu\text{m}$  size-fraction POC :  $^{234}\text{Th}$  values at  $z_{\text{PAR}}$  were significantly lower in the most equatorward zone north of  $45^\circ \text{S}$ , where average ratios were  $1.9 \pm 0.9 \mu\text{mol dpm}^{-1}$ . The highest average ratios, south of  $52^\circ \text{S}$ , were  $5.4 \pm 3.0 \mu\text{mol dpm}^{-1}$ , illustrating the wide variation in POC :  $^{234}\text{Th}$  ratios with ecosystem type (Buesseler et al., 2006; Jacquet et al., 2011). Likewise, zonally averaged POC export fluxes in the most equatorward zone ( $2.7 \pm 2.3 \text{ mmol m}^{-2} \text{ d}^{-1}$ ) were significantly lower than average fluxes in the most poleward zone ( $8.0 \pm 6.3 \text{ mmol m}^{-2} \text{ d}^{-1}$ ). BSi :  $^{234}\text{Th}$  values were significantly different in all three zones, with highest average ratios south of  $52^\circ \text{S}$  ( $7.1 \pm 4.1 \mu\text{mol dpm}^{-1}$ ) and smallest ratios north of  $45^\circ \text{S}$  ( $0.3 \pm 0.1 \mu\text{mol dpm}^{-1}$ ). Similarly, average BSi export fluxes were also significantly different from each other in all three zones, with the greatest average values south of  $52^\circ \text{S}$  ( $10 \pm 8.7 \text{ mmol m}^{-2} \text{ d}^{-1}$ ), and lowest values north of  $45^\circ \text{S}$  ( $0.35 \pm 0.16 \text{ mmol m}^{-2} \text{ d}^{-1}$ ). Finally, PIC :  $^{234}\text{Th}$  ratios, which averaged  $0.72 \pm 0.85 \mu\text{mol dpm}^{-1}$  across all zones, and PIC export fluxes were not significantly different from each other in any zone defined by these latitudinal bands.

**Table 3.** POC, biomineral, and  $^{234}\text{Th}$  concentrations and fluxes at  $z_{\text{PAR}}$ . Ez ratio is  $^{234}\text{Th}$ -derived POC flux at  $z_{\text{PAR}}$  divided by integrated primary productivity. The % > 51  $\mu\text{m}$  [POC] metric is the fraction of total [POC] in the > 51  $\mu\text{m}$  size fraction. POC and biomineral flux errors are propagated from  $^{234}\text{Th}$  flux, and POC :  $^{234}\text{Th}$  errors.

Cruise	Station	$z_{\text{PAR}}$	$^{234}\text{Th}$ flux	> 51 $\mu\text{m}$ [POC]	> 51 $\mu\text{m}$ [Bsi]	> 51 $\mu\text{m}$ [PIC]	> 51 $\mu\text{m}$ Th activity	POC : Th	POC flux	Bsi : Th	Bsi flux	PIC : Th	PIC flux	Primary productivity	Ez ratio	% > 51 $\mu\text{m}$ [POC]
–	–	m	$\text{dpm m}^{-2} \text{d}^{-1}$	$\mu\text{M}$	$\mu\text{M}$	$\mu\text{M}$	$\text{dpm L}^{-1}$	$\mu\text{mol dpm}^{-1}$	$\text{mmol m}^{-2} \text{d}^{-1}$	$\mu\text{mol dpm}^{-1}$	$\text{mmol m}^{-2} \text{d}^{-1}$	$\mu\text{mol dpm}^{-1}$	$\text{mmol m}^{-2} \text{d}^{-1}$	$\text{mmol m}^{-2} \text{d}^{-1}$	unitless	%
GB1	6	79	2437 ± 100	0.23 <sup>b</sup>	0.03 <sup>a</sup>	0.124 <sup>a</sup>	0.07 <sup>a</sup>	2.3 <sup>a</sup>	5.7 ± 0.26	0.4	0.9 ± 0.04	1.8	4.3 ± 0.20	42	0.14	8.8%
GB1	16	62	1933 ± 71	0.38	0.08	0.390	0.12	3.0	5.9 ± 0.68	0.6	1.2 ± 0.14	3.1	6.1 ± 0.70	165	0.04	17.7%
GB1	25	62	862 ± 46 <sup>a</sup>	0.04	0.005 <sup>a</sup>	0.015 <sup>a</sup>	0.02	1.8	1.6 ± 0.11	0.2	0.2 ± 0.02	0.7	0.6 ± 0.04	35	0.04	3.2%
GB1	32	69	1304 ± 116	0.07	0.01	0.027	0.04	1.8	2.3 ± 0.21	0.3	0.3 ± 0.03	0.7	0.9 ± 0.08	11	0.21	3.9%
GB1	38	121	809 ± 126	0.04	0.003	0.017	0.01	2.7	2.2 ± 0.35	0.2	0.2 ± 0.03	1.2	0.9 ± 0.15	21	0.10	8.4%
GB1	46	63	2123 ± 69	0.23	0.005	0.059	0.06	4.1	8.8 ± 0.38	0.1	0.2 ± 0.02	1.1	2.2 ± 0.10	13	0.67	5.3%
GB1	59	60	1844 ± 102	0.09	0.10	0.072	0.02	4.0	7.3 ± 0.52	4.6	8.6 ± 0.53	3.4	6.2 ± 0.39	26	0.28	5.3%
GB1	70	100	1280 ± 94	0.11	0.06 <sup>a</sup>	0.001 <sup>a</sup>	0.02	4.3	5.5 ± 0.44	3.5 <sup>a</sup>	4.5 ± 0.35	0.1 <sup>a</sup>	0.1 ± 0.09	10	0.53	10.6%
GB1	77	98	1485 ± 105	0.03	0.03	0.002	0.01	6.0	9.0 ± 1.3	5.6	8.3 ± 0.98	0.4	0.7 ± 0.23	57	0.16	3.6%
GB1	85	73	1858 ± 94	2.50	3.44	0.124	0.23	10.8	20 ± 1.1	14.9	28 ± 1.5	0.5	1.0 ± 0.05	53	0.38	52.0%
GB1	92	59	1639 ± 77	0.40	0.46	0.020	0.08	4.9	8.0 ± 0.40	5.6	9.3 ± 0.46	0.2	0.4 ± 0.02	26	0.31	11.3%
GB1	101	81	1763 ± 82	0.19	0.05	0.013	0.09	2.0	3.6 ± 0.18	0.5	0.9 ± 0.04	0.1	0.2 ± 0.01	22	0.17	12.5%
GB1	109	76	1524 ± 76	0.19 <sup>a</sup>	0.05 <sup>a</sup>	0.027 <sup>a</sup>	0.14 <sup>a</sup>	1.4	2.1 ± 0.11	0.4	0.6 ± 0.03	0.2	0.3 ± 0.02	14	0.16	21.0%
GB1	117	62	1177 ± 50	0.21	0.02	0.032	0.15	1.4	1.7 ± 0.07	0.1	0.2 ± 0.01	0.2	0.3 ± 0.01	18	0.09	6.6%
GB2	5	78	1889 ± 5207	0.08 <sup>b</sup>	0.01 <sup>a</sup>	0.048 <sup>a</sup>	0.05 <sup>a</sup>	1.6	3.0 ± 8.8	0.2	0.4 ± 1.2	1.0	1.9 ± 5.2	8.2	0.37	7.6%
GB2	27	105	1869 ± 160	0.08 <sup>a</sup>	0.10 <sup>a</sup>	0.060 <sup>a</sup>	0.04 <sup>a</sup>	1.9	3.5 ± 0.32	2.2	4.0 ± 0.35	1.3	2.5 ± 0.22	8.0	0.44	6.7%
GB2	36	90	988 ± 89	0.43	0.28	0.074	0.22	2.0	2.0 ± 0.18	1.3	1.3 ± 0.12	0.3	0.3 ± 0.03	12	0.16	15.6%
GB2	43	108	1221 ± 153	0.74 <sup>a</sup>	0.62 <sup>a</sup>	0.041 <sup>a</sup>	0.18 <sup>a</sup>	4.1	5.0 ± 0.63	3.4	4.2 ± 0.53	0.2	0.3 ± 0.04	12	0.43	37.8%
GB2	53	81	1058 ± 100 <sup>a</sup>	0.54 <sup>a</sup>	0.80 <sup>a</sup>	0.081 <sup>a</sup>	0.14 <sup>a</sup>	3.9	4.1 ± 0.40	5.7	6.1 ± 0.59	0.6	0.6 ± 0.07	16	0.25	22.5%
GB2	63	109	1229 ± 138	0.71 <sup>a</sup>	1.04 <sup>a</sup>	0.028 <sup>a</sup>	0.13 <sup>a</sup>	5.6 <sup>a</sup>	6.9 ± 0.78	8.1	9.9 ± 1.1	0.2	0.3 ± 0.03	9.0	0.77	33.2%
GB2	73	93	977 ± 108	0.21 <sup>b</sup>	1.13 <sup>a</sup>	0.014 <sup>a</sup>	0.20 <sup>a</sup>	3.3 <sup>a</sup>	3.2 ± 0.36	5.6	5.4 ± 0.60	0.1	0.1 ± 0.01	8.8	0.36	17.6%
GB2	87	107	1299 ± 115	0.06 <sup>b</sup>	0.30 <sup>a</sup>	0.041 <sup>a</sup>	0.06 <sup>a</sup>	2.5 <sup>a</sup>	3.2 ± 0.40	4.7	6.1 ± 0.55	0.6	0.8 ± 0.14	11	0.29	3.4%
GB2	93	113	1142 ± 137	0.07 <sup>a</sup>	0.01 <sup>a</sup>	0.023 <sup>a</sup>	0.05 <sup>a</sup>	1.3	1.5 ± 0.25	0.2	0.3 ± 0.06	0.4	0.5 ± 0.14	12	0.12	4.3%
GB2	100	113	1112 ± 130	0.08	0.02	0.006	0.06	1.4	1.5 ± 0.19	0.3	0.3 ± 0.04	0.1	0.1 ± 0.02	14	0.11	12.8%
GB2	106	102	1394 ± 82 <sup>a</sup>	0.09 <sup>b</sup>	0.04 <sup>a</sup>	0.024 <sup>a</sup>	0.12 <sup>a</sup>	0.8	1.1 ± 0.86	0.3 <sup>a</sup>	0.4 ± 0.02	0.2	0.3 ± 0.02	22	0.05	12.2%
GB2	112	76	717 ± 97	0.22 <sup>b</sup>	0.17 <sup>a</sup>	0.087 <sup>a</sup>	0.36 <sup>a</sup>	1.4 <sup>a</sup>	1.0 ± 0.13	0.5	0.3 ± 0.05	0.2	0.2 ± 0.02	no data	no data	13.3%
GB2	119	92	1223 ± 124	0.51 <sup>a</sup>	0.12 <sup>a</sup>	0.048 <sup>a</sup>	0.22 <sup>a</sup>	2.3	2.8 ± 0.29	0.5	0.7 ± 0.07	0.2	0.3 ± 0.03	17	0.17	21.5%

<sup>a</sup> Values at  $z_{\text{PAR}}$  estimated by linear interpolation of values at upper and lower depths around  $z_{\text{PAR}}$ . <sup>b</sup> > 51  $\mu\text{m}$  [POC] values interpolated by significant power-law fits (Fig. 3). "no data": not enough depths were sampled and analyzed to interpolate at  $z_{\text{PAR}}$ .

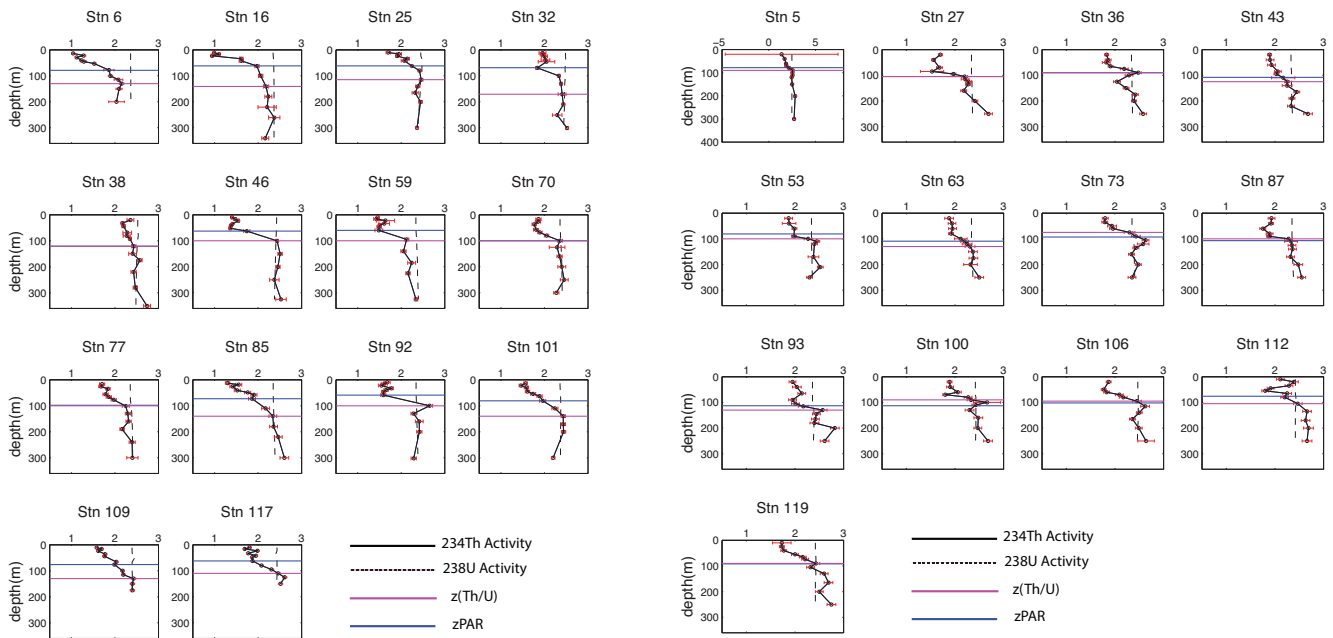


**Figure 4.** Total  $^{234}\text{Th}$  and  $^{238}\text{U}$  activity profiles measured at 14 stations of GB1 and 13 stations of GB2 (note different x axis for station GB2-5; Table S1). Error bars for  $^{234}\text{Th}$  activity are propagated errors.  $^{238}\text{U}$  is calculated from salinity. All  $^{234}\text{Th}$  activity profiles exhibit a deficit relative to  $^{238}\text{U}$  activity at the surface, and mostly return to equilibrium with  $^{238}\text{U}$  within error at depth of  $z_{\text{Th/U}}$  (Table 1). Refer to Fig. 1 for station locations.

These fluxes are sensitive to the choice of export depth ( $z_{\text{PAR}}$  or  $z_{\text{Th/U}}$ ), not only because the export depth determines the magnitude of  $^{234}\text{Th}$  flux by influencing the integrated  $^{234}\text{Th}$  deficit but also because the export depth determines which POC :  $^{234}\text{Th}$  ratio best describes particles sinking from the chosen depth (Fig. S1). Across stations, the

depth metrics  $z_{\text{PAR}}$  and  $z_{\text{Th/U}}$  differed from each other to varying extents (Fig. 4; Table 1). As exemplified by stations GB1-92, GB1-16, and GB2-100, POC fluxes changed significantly between  $z_{\text{PAR}}$  and  $z_{\text{Th/U}}$  (Fig. 5b, c; Table S2). At station GB1-92, where  $z_{\text{PAR}}$  was 40 m shallower than  $z_{\text{Th/U}}$ , POC flux decreased from 8.0 at  $z_{\text{PAR}}$  to 5.1  $\text{mmol m}^{-2} \text{d}^{-1}$

**Table 4.** Mean  $\pm$  standard deviations of  $^{234}\text{Th}$  fluxes, POC :  $^{234}\text{Th}$ , BSi :  $^{234}\text{Th}$ , PIC :  $^{234}\text{Th}$ , POC fluxes, and biomineral fluxes at  $z_{\text{PAR}}$ , divided by three latitude zones.  $45^\circ\text{S}$  marks the approximate latitude of the Subantarctic Front, while  $52^\circ\text{S}$  marks the approximate latitude of the polar front (Belkin and Gordon, 1996; Sokolov and Rintoul, 2009).

Lat. zone	$^{234}\text{Th}$ flux at $z_{\text{PAR}}$	POC : Th at $z_{\text{PAR}}$	POC flux at $z_{\text{PAR}}$	BSi : Th at $z_{\text{PAR}}$	BSi flux at $z_{\text{PAR}}$	PIC : Th at $z_{\text{PAR}}$	PIC flux at $z_{\text{PAR}}$	No. of stns.
$^\circ\text{S}$	$\text{dpm m}^{-2} \text{d}^{-1}$	$\mu\text{mol dpm}^{-1}$	$\text{mmol m}^{-2} \text{d}^{-1}$	$\mu\text{mol dpm}^{-1}$	$\text{mmol m}^{-2} \text{d}^{-1}$	$\mu\text{mol dpm}^{-1}$	$\text{mmol m}^{-2} \text{d}^{-1}$	–
36–45	$1.3 \pm 0.44$	$1.9 \pm 0.9$	$2.7 \pm 2.3$	$0.3 \pm 0.1$	$0.33 \pm 0.17$	$0.5 \pm 0.4$	$0.73 \pm 0.76$	10
45–52	$1.5 \pm 0.50$	$2.8 \pm 1.2$	$4.4 \pm 2.2$	$2.3 \pm 2.2$	$3.4 \pm 3.3$	$1.1 \pm 1.2$	$2.0 \pm 2.4$	11
52–>60	$1.4 \pm 0.30$	$5.4 \pm 3.0$	$8.0 \pm 6.3$	$7.1 \pm 4.1$	$10 \pm 8.7$	$0.3 \pm 0.2$	$0.49 \pm 0.4$	6

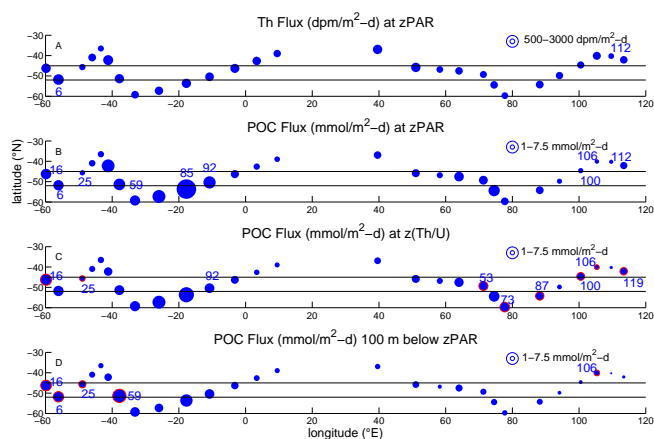


**Figure 5.** Distribution of  $^{234}\text{Th}$  flux and  $^{234}\text{Th}$ -derived POC flux at 27 stations along GB1 and GB2 (circle area scales with flux magnitude). (a)  $^{234}\text{Th}$  fluxes at  $z_{\text{PAR}}$  range from  $717 \text{ dpm m}^{-2} \text{d}^{-1}$  at station GB2-112 to  $2437 \text{ dpm m}^{-2} \text{d}^{-1}$  at GB1-6. (b) POC fluxes at  $z_{\text{PAR}}$  range from  $0.97 \text{ mmol m}^{-2} \text{d}^{-1}$  at station GB2-112 to  $20 \text{ mmol m}^{-2} \text{d}^{-1}$  at GB1-85. (c) POC fluxes at  $z_{\text{Th/U}}$  range from  $0.57 \text{ mmol m}^{-2} \text{d}^{-1}$  at station GB2-112 to  $12 \text{ mmol m}^{-2} \text{d}^{-1}$  at GB1-85 (Table S2). (d) POC fluxes at 100 m below  $z_{\text{PAR}}$  range from  $0.23 \text{ m}^{-2} \text{d}^{-1}$  at station GB2-112 to  $9.5 \text{ mmol m}^{-2} \text{d}^{-1}$  at GB1-59. A few station numbers discussed in the text are indicated. Red outlines distinguish stations where fluxes are greater at the specified depth than at  $z_{\text{PAR}}$ . The two horizontal dashed lines at  $45$  and  $52^\circ\text{S}$  represent the approximate locations of the Subantarctic and polar fronts, respectively (Belkin and Gordon, 1996; Sokolov and Rintoul, 2009). Refer to Fig. 1 for other station locations.  $z_{\text{PAR}}$  and  $z_{\text{Th/U}}$  are defined as in Table 1.

at  $z_{\text{Th/U}}$ . In contrast, at station GB1-16, where  $z_{\text{PAR}}$  was  $80 \text{ m}$  shallower than  $z_{\text{Th/U}}$ , POC fluxes increased from  $5.9$  to  $6.6 \text{ mmol m}^{-2} \text{d}^{-1}$ . At station GB2-100, one of few stations where  $z_{\text{PAR}}$  was deeper than  $z_{\text{Th/U}}$ , POC fluxes decreased from  $3.3$  to  $1.5 \text{ mmol m}^{-2} \text{d}^{-1}$  going deeper. At this station, the POC :  $^{234}\text{Th}$  ratio at  $z_{\text{Th/U}}$  was  $102\%$  greater than ratios at  $z_{\text{PAR}}$ , while  $^{234}\text{Th}$  fluxes at  $z_{\text{Th/U}}$  were  $6\%$  greater than fluxes at  $z_{\text{PAR}}$ , demonstrating that changes in particle composition disproportionately contributed to the observed difference in POC export at  $z_{\text{PAR}}$  and  $z_{\text{Th/U}}$ . By contrast, at station GB1-16, the relative change in  $^{234}\text{Th}$  fluxes from  $z_{\text{PAR}}$

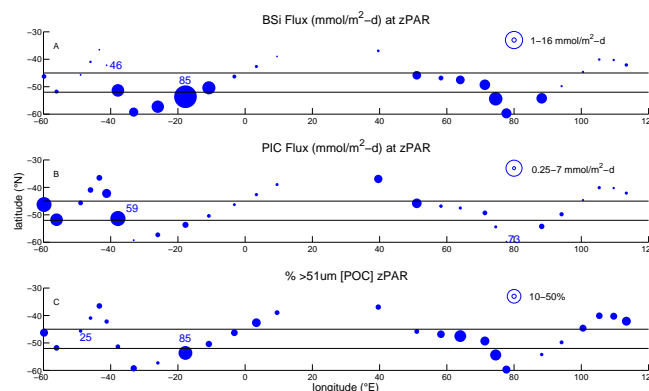


**Figure 6.** Distribution of BSi flux, PIC flux, and  $\% > 51 \mu\text{m} [\text{POC}]$ , the percent of total  $[\text{POC}]$  in the  $> 51 \mu\text{m}$  size class, at  $z_{\text{PAR}}$  (Table 1) along GB1 and GB2 (circle area scales with magnitude). (a) BSi fluxes range from  $0.17 \text{ mmol m}^{-2} \text{d}^{-1}$  at station GB1-46 to  $28 \text{ mmol m}^{-2} \text{d}^{-1}$  at GB1-85. (b) PIC fluxes range from  $0.067 \text{ mmol m}^{-2} \text{d}^{-1}$  at station GB2-73 to  $6.2 \text{ mmol m}^{-2} \text{d}^{-1}$  at GB2-59. (c) The proportion of  $[\text{POC}]$  in the  $> 51 \mu\text{m}$  size fraction at  $z_{\text{PAR}}$  ranges from  $3.3\%$  at station GB1-25 to  $52\%$  at GB1-85. A few station numbers discussed in the text are indicated. The two horizontal dashed lines at  $45$  and  $52^\circ\text{S}$  represent the approximate locations of the Subantarctic and polar fronts, respectively (Belkin and Gordon, 1996; Sokolov and Rintoul, 2009). Refer to Fig. 1 for other station locations.

to  $z_{\text{Th/U}}$  ( $+29\%$ ) contributed more to the increase in POC flux with depth than the relative change in POC :  $^{234}\text{Th}$  ratio ( $-13\%$ ). Finally, for station GB1-92, the relative change in  $^{234}\text{Th}$  flux with depth ( $-19\%$ ) was similar to the relative change in POC :  $^{234}\text{Th}$  with depth ( $-21\%$ ), demonstrating that the export flux estimate was equally sensitive to changes in both parameters.

#### 4 Discussion

The following discusses these flux measurements in the context of other Southern Ocean observations, as well as hypotheses surrounding the transformation of sinking organic carbon within the euphotic and mesopelagic zones of the water column.

#### 4.1 Choice of export depth

The two possible depths we use to calculate export flux,  $z_{\text{PAR}}$  and  $z_{\text{Th/U}}$ , are significantly different in the Atlantic sector, which influences the magnitude of flux estimated (see Sect. 3). We offer here two possible and not mutually exclusive explanations for why  $z_{\text{Th/U}}$  depths were on average deeper than  $z_{\text{PAR}}$  depths at GB1 stations.

One hypothesis is that the  $^{234}\text{Th}$ – $^{238}\text{U}$  profiles used to calculate export fluxes may not have been at steady state during the time of sampling on the GB1 cruise. Non-steady-state conditions in the  $^{238}\text{U}$ – $^{234}\text{Th}$  system do occur during phytoplankton blooms, particularly during their decline and ascent (Savoye et al., 2006; Buesseler et al., 2009). For example, a recent and rapid increase in the near-surface particle concentration could decrease the depth of light penetration faster than the  $^{238}\text{U}$ – $^{234}\text{Th}$  system can adjust, leading to a  $z_{\text{PAR}}$  measured on station that is shallower than the  $z_{\text{Th/U}}$ , which reflects conditions prior to the rapid increase. Since the GB1 cruise in the Atlantic sector took place a month earlier in the growing season (January–February 2011) than the GB2 cruise in the Indian sector (February–March 2012), the two sectors may have been sampled at different stages of the seasonal bloom, contributing to differences in agreement between  $z_{\text{PAR}}$  and  $z_{\text{Th/U}}$ . Satellite chlorophyll time series, if well resolved, can shed light on how dynamic primary production was around the time of sampling at each station of GB1 and GB2, whether rapid (i.e., within 3 weeks) changes in particle production and sinking fluxes from a bloom could have decoupled  $^{234}\text{Th}$ – $^{238}\text{U}$  deficits from light profiles into the surface ocean of the Great Calcite Belt. Eight-day composites of chlorophyll imagery from December 2010 to February 2011 were required to overcome spatial patchiness in the data due to clouds, and these indicate that the changes leading up to sampling during GB1 were not consistent across all stations where  $z_{\text{PAR}} < z_{\text{Th/U}}$ . At several stations, chlorophyll concentrations declined towards the sampling date; at others, chlorophyll did not change or increased towards the sampling date. Moreover, out of the three stations where  $z_{\text{PAR}} = z_{\text{Th/U}}$ , only one exhibited relatively constant chlorophyll concentrations in the month preceding sampling. In GB2, where the differences between  $z_{\text{PAR}}$  and  $z_{\text{Th/U}}$  were not significant, chlorophyll tended to be constant preceding more sampling stations. Nonetheless, as in GB1, several locations still experienced increasing or decreasing chlorophyll concentrations in the weeks before sampling, despite having a similar  $z_{\text{PAR}}$  and  $z_{\text{Th/U}}$ .

The inability of the chlorophyll time series to unequivocally resolve the differences between  $z_{\text{PAR}}$  and  $z_{\text{Th/U}}$  points to other possible mechanisms underlying the discrepancy. One other mechanism, which does not necessarily preclude non-steady state in the  $^{234}\text{Th}$  system, is sinking particle production below the euphotic zone  $z_{\text{PAR}}$  (Trull et al., 2008). Physical aggregation and fecal pellet production by zooplankton grazing in the region below  $z_{\text{PAR}}$  (i.e., the upper

mesopelagic zone) can increase the speed and total abundance of sinking of particles by transforming phytoplankton biomass exiting the euphotic zone, thereby contributing to sustained  $^{234}\text{Th}$  deficits below  $z_{\text{PAR}}$  (Steinberg et al., 2008; Wilson et al., 2008; Abramson et al., 2010). Why this occurs only in GB1 and not GB2 is not known.

For example, the  $\sim 70$  m difference in  $z_{\text{PAR}}$  and  $z_{\text{Th/U}}$  at a station like GB1-85 (Table 1) may be attributed to additional production or repackaging of sinking particles in the upper mesopelagic zone, causing  $^{234}\text{Th}$  deficits to persist beyond the euphotic zone of primary productivity, and a deeper  $z_{\text{Th/U}}$ . Images of  $> 51 \mu\text{m}$  particles from this station highlight the changing nature of  $> 51 \mu\text{m}$  particles with depth (Fig. 2), from primarily large phytoplankton in the euphotic zone to predominantly fecal pellets in the mesopelagic zone. The difference in POC fluxes measured at both depths may arise from the evolution of these particles during vertical transit, from predominantly intact and relative buoyant diatoms at  $z_{\text{PAR}}$  to degraded, sinking fecal pellets produced between  $z_{\text{PAR}}$  and  $z_{\text{Th/U}}$ .

Going forward, it is most important to keep in mind how the choice of export depth impacts flux estimates. For this study, all export fluxes are defined by  $z_{\text{PAR}}$  so that they can be compared with integrated primary production measurements (Buesseler and Boyd, 2009). Non-steady-state effects of  $^{234}\text{Th}$  profiles on export fluxes will not be considered further because we do not have Lagrangian observations at multiple time points necessary to detect such effects (Buesseler et al., 2003; Resplandy et al., 2012).

#### 4.2 Comparison of export fluxes to previous studies

The  $^{234}\text{Th}$  fluxes we report (mean  $\pm$ SD =  $1413 \pm 432 \text{ dpm m}^{-2} \text{ d}^{-1}$ ) are generally within range of measurements from other Southern Ocean studies ( $1615 \pm 1050 \text{ dpm m}^{-2} \text{ d}^{-1}$ ; compilation by Le Moigne et al., 2013; Shimmield et al., 1995; Rutgers Van Der Loeff et al., 1997, 2011; Buesseler, 1998; Cochran et al., 2000; Buesseler et al., 2001, 2003; Friedrich and van der Loeff, 2002; Coppola et al., 2005; Morris et al., 2007; Thomalla et al., 2008; Savoye et al., 2008; Rodriguez y Baena et al., 2008; Jacquet et al., 2011; Zhou et al., 2012; Planchon et al., 2013). By contrast, the POC fluxes we report ( $4.5 \pm 3.9 \text{ mmol m}^{-2} \text{ d}^{-1}$ ) are on average 3 times lower than fluxes from other studies ( $12.6 \pm 13.3 \text{ mmol m}^{-2} \text{ d}^{-1}$ ) due to lower POC :  $^{234}\text{Th}$  ratios measured in  $> 51 \mu\text{m}$  particles. In general, POC :  $^{234}\text{Th}$  ratios can vary widely as a function of season, ecosystem composition, size fraction, depth, and particle sampling methodology (Coppola et al., 2005; Buesseler et al., 2006; Santschi et al., 2006; Jacquet et al., 2011). In GB1 and GB2, an ecosystem effect likely accounts for the 14-fold difference in POC :  $^{234}\text{Th}$  between oligotrophic waters (e.g.,  $0.8 \mu\text{mol dpm}^{-1}$  at GB2-106) and polar waters (e.g.,  $10.8 \mu\text{mol dpm}^{-1}$  at GB1-85; Table 3). The Le Moigne et al. (2013) data set may include more

studies from diatom-rich ecosystems with high POC :  $^{234}\text{Th}$  organic particles, such as observed by Buesseler (1998; not included in Le Moigne et al., 2013), driving some of the discrepancy between our observations and POC fluxes reported by (Le Moigne et al., 2012).

Other potential reasons for POC :  $^{234}\text{Th}$  differences are the choice of export depth (see Sect. 4.1) and different sampling methodologies in the previous studies. For instance, in situ pump filter holders with a small-diameter central intake and thus higher intake velocities have been observed to sample more zooplankton, which typically have higher POC :  $^{234}\text{Th}$  ratios, than filter holders with diffuse intakes (Bishop et al., 2012). This is because swimming zooplankton can avoid the gentle intake velocities of filter holders with diffuse intakes but not the higher velocities of small diameter intakes. This would be expected to affect estimates of  $^{234}\text{Th}$ -derived POC flux more than  $^{234}\text{Th}$ -derived biomineral fluxes.

There have been far fewer estimates of  $^{234}\text{Th}$ -derived biomineral export fluxes (Thomalla et al., 2008; Sanders et al., 2010; Le Moigne et al., 2012, 2013). BSi and PIC fluxes observed during GB1 and GB2 are within the range previously observed during the Crozet study by the Crozet Islands (Le Moigne et al., 2012), the site of station GB2-27. Thomalla et al. (2008) also reported biomineral fluxes from the Atlantic Meridional Transect (AMT), north of the Subantarctic Front. While AMT PIC export fluxes were only 2 times smaller than our mean PIC fluxes in the Great Calcite Belt region, AMT BSi fluxes were 10 times smaller. The disparity in BSi fluxes is unsurprising, since the AMT cruise track was through waters with a low abundance of silicifiers. We also find that the PIC and BSi fluxes from our Great Calcite Belt study are 4 and 10 times larger, respectively, than biomineral fluxes estimated by Henson et al. (2012b), who used a steady-state model of nutrient uptake against nutrient export (Sarmiento et al., 2002, 2004). The Henson et al. method used annual climatologies of nutrient concentration profiles for their estimates, whereas the  $^{234}\text{Th}$ -derived export method used here integrates over several weeks in the growing season. This difference in timescales of integration likely accounts for the smaller biomineral fluxes in Henson et al. (2012b).

### 4.3 Export efficiency

We found no significant relationship observed between integrated primary productivity and POC flux at  $z_{\text{PAR}}$ , highlighting the variable export efficiency across GB1 and GB2. Export efficiencies, or “Ez ratios” (Buesseler and Boyd, 2009), were calculated as the ratio of POC flux at  $z_{\text{PAR}}$  to total integrated primary production in the euphotic zone (Fig. 7b; Table 3). Mean export efficiencies were  $0.26 \pm 0.19$ , and ranged from 0.04 at station GB1-16 to 0.77 at GB2-63. The lack of association between primary productivity and POC export flux confirms previously observed decoupling between the factors that drive export and those that modulate primary pro-

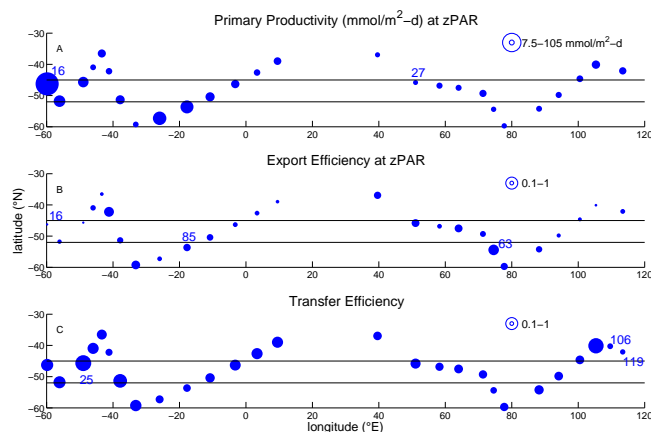


**Figure 7.** Distribution of primary productivity, export efficiency, and transfer efficiency along GB1 and GB2 (circle area scales with magnitude). (a) Primary productivity integrated through the euphotic zone ranges from  $8.0 \text{ mmol m}^{-2} \text{ d}^{-1}$  at station GB2-27 to  $165 \text{ mmol m}^{-2} \text{ d}^{-1}$  at GB1-16. (b) Export efficiency ( $E_z$  ratio) at  $z_{\text{PAR}}$  to primary productivity integrated to  $z_{\text{PAR}}$ , ranges from 0.04 at station GB1-16 to 0.77 at GB2-63. (c) Transfer efficiency at  $z_{\text{PAR}}$ , which is the ratio of POC flux 100 m below  $z_{\text{PAR}}$  to POC flux at  $z_{\text{PAR}}$ , ranges from 0.20 at station GB1-119 to 1.8 at GB1-25. A few station numbers discussed in the text are indicated. The two horizontal dashed lines at 45 and 52° S represent the approximate locations of the Subantarctic and polar fronts, respectively (Belkin and Gordon, 1996; Sokolov and Rintoul, 2009). Refer to Fig. 1 for other station locations.

ductivity (Buesseler et al., 2001; Coppola et al., 2005; Maiti et al., 2012).

### 4.4 Vertical attenuation of POC flux and concentration

At most stations, both POC flux and  $> 51 \mu\text{m}$  [POC] decline with depth below  $z_{\text{PAR}}$  as a result of remineralization. In the following, we use two metrics to describe POC transfer in the mesopelagic zone: (1) the attenuation of  $> 51 \mu\text{m}$  [POC] in the mesopelagic zone, expressed as the attenuation coefficients extracted from power-law fits of mesopelagic  $> 51 \mu\text{m}$  [POC] (exponent from Eq. 1) and (2) the POC flux transfer efficiency ( $T_{100}$ ), defined as the fraction of  $^{234}\text{Th}$ -based POC flux that survives remineralization and is transferred 100 m below  $z_{\text{PAR}}$  (Buesseler and Boyd, 2009). The first metric describes the disappearance of POC concentration, and applies to the entire mesopelagic zone; the second metric describes the survival of POC flux, and applies to the upper mesopelagic zone.

The mean  $T_{100}$  was  $0.71 \pm 0.38$ , ranging from 0.20 at station GB2-119 to 1.8 at GB1-25 (Fig. 7c; Table 2), generally falling within the spread of values observed globally as well as specifically in the Southern Ocean (Buesseler and Boyd, 2009). At stations GB1-6, GB1-16, GB1-25, GB1-59, and GB2-106,  $T_{100}$  values are greater than 1.0 and reflect an in-

crease in POC flux with depth between  $z_{\text{PAR}}$  and 100 m below  $z_{\text{PAR}}$  (Fig. 5b, d). Transfer efficiencies greater than 1 can occur during a declining bloom (Henson et al., 2015), but examination of satellite chlorophyll time series does not indicate that these stations were sampled at such conditions. At GB1-6, GB1-16, and GB1-59, the  $^{234}\text{Th}$ – $^{238}\text{U}$  disequilibrium extends relatively deep (>200m) into the water column, thus leading to continually increasing  $^{234}\text{Th}$  flux with depth, suggesting that either renewed particle production at depth or lateral advection of particles away from these coastal stations could sustain the  $^{234}\text{Th}$  deficit below  $z_{\text{PAR}}$ . Moreover, because  $z_{\text{PAR}}$  depths are significantly shallower than  $z_{\text{Th/U}}$  in most GB1 stations, including GB1-6, GB1-16, and GB1-59, the transfer efficiency calculation at these stations in GB1 captures an increase in  $^{234}\text{Th}$  flux between  $z_{\text{PAR}}$  and 100 m below  $z_{\text{PAR}}$ . Thus, for the following discussion, it is important to view transfer efficiency values with the caveat that GB1 and GB2 stations display different  $^{234}\text{Th}$ – $^{238}\text{U}$  disequilibrium profiles with respect to  $z_{\text{PAR}}$  and  $z_{\text{Th/U}}$ , and this difference impacts all calculations that use a  $^{234}\text{Th}$  flux component.

At the two other stations for which  $T_{100} > 1$ , GB1-25 and GB2-106, the increases in POC flux below  $z_{\text{PAR}}$  arise primarily from increasing POC :  $^{234}\text{Th}$  ratios rather than increasing  $^{234}\text{Th}$  flux with depth (Fig. S1a, d in the Supplement). The increase in these ratios results from a faster decrease in particulate  $^{234}\text{Th}$  activity compared to changes in  $>51\ \mu\text{m}$  [POC] with depth. This is unexpected, and at all other stations,  $>51\ \mu\text{m}$  [POC] decreases more quickly than particulate  $^{234}\text{Th}$  activity due to organic carbon remineralization. We suspect that poor  $>51\ \mu\text{m}$  particle distribution on filters from GB2-106 may have led to anomalously low POC around  $z_{\text{PAR}}$ , but we do not have an explanation for the consistent increase in POC : Th with depth at GB1-25 (Fig. S1a). We proceed by excluding the  $T_{100}$  transfer efficiencies from these two stations from statistical tests, but we identify them for completeness (Figs. 7, 9).

The general decline in POC flux with depth at most stations is mirrored by a decrease in  $>51\ \mu\text{m}$  [POC], both of which are a result of remineralization. Attenuation coefficients from power-law fits of mesopelagic  $>51\ \mu\text{m}$  [POC] at 22 stations describe this transformation from  $z_{\text{PAR}}$  to the lower mesopelagic zone, where  $>51\ \mu\text{m}$  [POC] between 800 and 1000 m was 1.5 to 137 times lower than  $>51\ \mu\text{m}$  [POC] at  $z_{\text{PAR}}$  (Fig. 8b, c; Table 2). We discount the attenuation value at station GB2-93 from discussion because it had an anomalously low  $>51\ \mu\text{m}$  [POC] at 800 m, likely due to incomplete rinsing of particles from the prefilter. This drove the power-law fit to yield an anomalously high attenuation coefficient, an outlier, as approximated by Chauvenet's theorem (Glover et al., 2011). Attenuation coefficients were  $1.1 \pm 0.50$  on average, and varied from 0.4 at station GB1-25 to 1.9 at GB2-43 (Fig. 8c; Table 2), which spans the global range compiled by Lam et al. (2011).

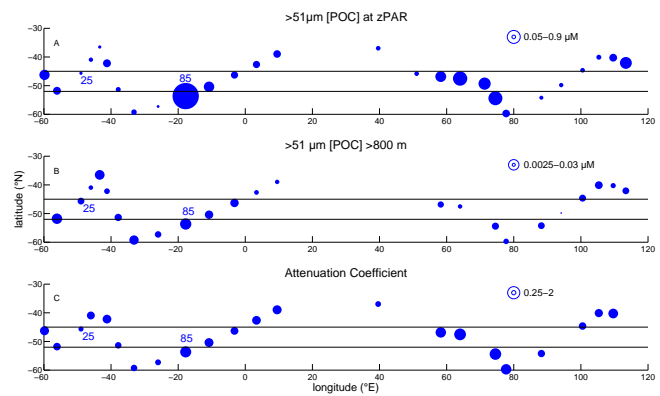


**Figure 8.** Distribution and vertical attenuation coefficient of  $>51\ \mu\text{m}$  [POC] (circle area scales with magnitude). (a)  $>51\ \mu\text{m}$  POC concentrations at  $z_{\text{PAR}}$  (Table 1) range from 0.03 at station GB1-77 to  $2.5\ \mu\text{M}$  at GB1-85. (b)  $>51\ \mu\text{m}$  [POC] at the deepest pump depth in the lower mesopelagic zone (800–1000 m). Concentrations range from 0.001 at station GB2-93 to  $0.035\ \mu\text{M}$  at GB1-85. (c) Attenuation coefficient from significant power-law fits of 22  $>51\ \mu\text{m}$  [POC] profiles, excluding GB2-93 (see Sect. 4.4). A few station numbers discussed in the text are indicated. The two horizontal dashed lines at 45 and 52° S represent the approximate locations of the Subantarctic and polar fronts, respectively (Belkin and Gordon, 1996; Sokolov and Rintoul, 2009). Refer to Fig. 1 for other station locations.

The  $>51\ \mu\text{m}$  [POC] at  $z_{\text{PAR}}$  is not correlated with  $>51\ \mu\text{m}$  [POC] at lower mesopelagic depths, suggesting that processes controlling  $>51\ \mu\text{m}$  [POC] at the top of the mesopelagic differ from those controlling  $>51\ \mu\text{m}$  [POC] at the base of the mesopelagic zone. This is supported by the great variation in attenuation coefficients and transfer efficiencies, and suggests that POC concentrations at  $z_{\text{PAR}}$  are decoupled from [POC] at  $z \geq 800\ \text{m}$ , as has also been noted in other POC flux and concentration observations (Lomas et al., 2010; Lam et al., 2011; Henson et al., 2012b). There are some exceptions, such as at GB1-85, which exhibited the highest  $>51\ \mu\text{m}$  [POC] both at  $z_{\text{PAR}}$  and below 800 m, but there is no overall relationship across the data set. The remaining discussion aims to tease apart the processes that control POC flux and  $>51\ \mu\text{m}$  [POC] in each depth regime.

#### 4.5 Biomineral–POC flux correlations at $z_{\text{PAR}}$

We compared POC fluxes to mineral fluxes at  $z_{\text{PAR}}$  (Fig. 9a, b) to test the hypothesis that mineral ballasting facilitates POC export out of the euphotic zone, as has been observed in deeper flux data sets  $>1000\ \text{m}$  (Klaas and Archer, 2002; Armstrong et al., 2002; Francois et al., 2002). Because we use  $^{234}\text{Th}$  activity deficits and the same particulate  $^{234}\text{Th}$  activities to derive all fluxes (Eq. 4–6), comparing export fluxes is equivalent to comparing concentrations of  $>51\ \mu\text{m}$  POC, BSi, and PIC at  $z_{\text{PAR}}$ . In this data set, minor differences between flux versus concentration comparisons (not

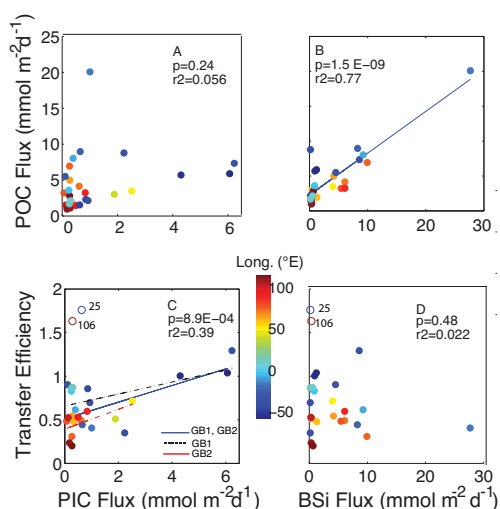


**Figure 9.**  $^{234}\text{Th}$ -derived POC flux as a function of (a) PIC flux and (b) BSi flux at  $z_{\text{PAR}}$ . POC flux transfer efficiency between  $z_{\text{PAR}}$  and  $z_{\text{PAR}}+100\text{ m}$  ( $T_{100}$ , defined in Sect. 4.4) as a function of (c) PIC flux and (d) BSi flux at  $z_{\text{PAR}}$ . Significant linear relationships are plotted as a solid blue line.  $T_{100}$  values at GB1-25 and GB2-106 were excluded from all correlations (Sect. 4.4). The color bar indicates the longitude of GB1 and GB2 stations. Refer to Fig. 1 for more specific station locations.

shown) arise from differences in interpolation methods for POC :  $^{234}\text{Th}$ , BSi :  $^{234}\text{Th}$ , and PIC :  $^{234}\text{Th}$  ratios at  $z_{\text{PAR}}$  (Table 3).

Pearson correlation tests between shallow POC export and the two biomineral fluxes revealed a significantly positive correlation between POC and BSi fluxes ( $p < 0.001$ ,  $r^2 = 0.77$ ). By contrast, there was no significant relationship between shallow POC and PIC fluxes ( $p = 0.24$ ,  $r^2 = 0.06$ ). Both BSi and POC export fluxes tend to increase poleward from the region north of the subtropical/Subantarctic Front to the inter-frontal zone to the region south of the polar front (Figs. 5b, 6a, b). Station GB1-85, which sits just south of the polar front ( $\sim 52^\circ\text{ S}$ ), is a high BSi and POC flux outlier. When removed, the BSi flux vs. POC flux correlation remains significant, though weaker ( $r^2 = 0.43$ ), suggesting that although this correlation is strongly influenced by station GB1-85, the shallow BSi ballast association still remains valid for the rest of the data set.

We also compared POC export fluxes to both PIC and BSi export fluxes simultaneously by multiple linear regression:

$$\text{POC Flux} = (m_{\text{BSi}} \cdot \text{BSi Flux}) + (m_{\text{PIC}} \cdot \text{PIC Flux}) + \text{constant}. \quad (7)$$

The multiple linear regression only explains an additional 5% of the variance in POC flux at  $z_{\text{PAR}}$  ( $r^2 = 0.82$ ,  $p < 0.001$ ), affirming that BSi flux explains most of the variation in POC export fluxes at  $z_{\text{PAR}}$  across the Atlantic and Indian sectors of the Great Calcite Belt region.

The per-mole carrying capacities of BSi and PIC for POC, or the slopes  $m_{\text{BSi}}$  and  $m_{\text{PIC}}$  in the multiple linear regression Eq. (7), are 0.60 and 0.50, respectively. The per-weight carrying capacities of BSi and PIC for POC are 0.23 and 0.13, respectively, assuming  $12 \times 2.199\text{ g mol}^{-1}$  POC,  $67.3\text{ g SiO}_2 \cdot 0.4\text{H}_2\text{O mol}^{-1}$  BSi, and  $100.1\text{ g CaCO}_3\text{ mol}^{-1}$  PIC (Klaas and Archer, 2002). The unassociated POC flux, the constant in Eq. (7), is  $1.7\text{ mmol POC m}^{-2}\text{ d}^{-1}$ , or  $44\text{ mg POC m}^{-2}\text{ d}^{-1}$ . These carrying capacities for POC are 2–10 times higher than global biomineral carrying capacities of deeper ( $> 2000\text{ m}$ ) flux data ( $m_{\text{BSi}} = 0.025\text{--}0.026$ ,  $m_{\text{PIC}} = 0.070\text{--}0.074$ ; Klaas and Archer, 2002), reflecting how POC remineralization with depth consistently reduces apparent mineral carrying capacities between the base of the euphotic zone and the deep sea.

These upper ocean carrying capacities, especially  $m_{\text{PIC}}$ , are considerably different than corresponding per-weight carrying capacities reported in the Crozex study in the Indian sector of the Southern Ocean ( $m_{\text{BSi}} = 0.16$ ,  $m_{\text{PIC}} = -0.11$ , constant =  $105\text{ mg POC m}^{-2}\text{ d}^{-1}$ ; Le Moigne et al., 2012). But, as the Crozex study was carried out several months earlier in the growing season than our sampling of the same area within the Great Calcite Belt, seasonal changes in the phytoplankton communities and their associated food webs could account for the differences in upper ocean carrying capacities. The study of Le Moigne et al. (2012) also highlighted that variable ecosystem composition contributed to regional variations in upper ocean carrying capacities (Le Moigne et al., 2014), echoing a contemporaneous study that showed that even the deep ( $> 1500\text{ m}$ ) flux carrying capacities have statistically significant spatial variability (Wilson et al., 2012).

It is worth noting that Le Moigne et al. (2012) included lithogenic minerals in their multiple linear regressions. We did not measure lithogenic minerals on GB1 and GB2, as we assumed lithogenic fluxes to be small in the Southern Ocean due to low terrestrial dust inputs (e.g., Honjo et al., 2000). While omitting this lithogenic component from the multiple linear regression could potentially impact derived  $m_{\text{BSi}}$  and  $m_{\text{PIC}}$  values, lithogenic material is nonetheless unlikely to be an important carrier of POC flux because of its low flux in the Southern Ocean. Indeed, regional studies have found that the lithogenic carrying capacity (Wilson et al., 2012) and the lithogenic-associated POC fluxes (Le Moigne et al., 2012) are very low in the Southern Ocean.

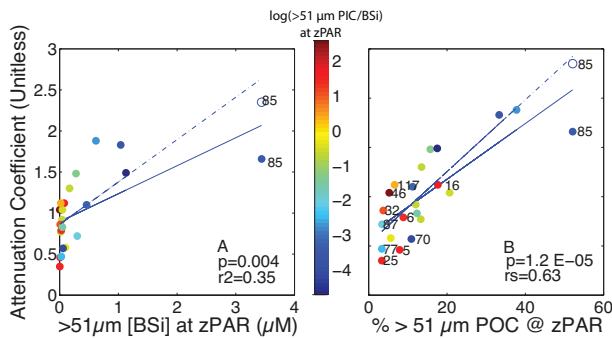


**Figure 10.** Attenuation coefficient as a function of (a)  $>51 \mu\text{m}$  [BSi] at  $z_{\text{PAR}}$  and (b) the proportion of [POC] in the  $>51 \mu\text{m}$  size fraction at  $z_{\text{PAR}}$ . The open circle indicates where GB1-85 would plot with a higher attenuation coefficient of 2.35, derived from fitting  $>51 \mu\text{m}$  [POC] at depths between  $z_{\text{PAR}}$  and 500 m. Significant linear relationships using the lower and higher attenuation coefficient values for GB1-85 are shown as solid and dashed lines, respectively;  $p$  and  $r^2$  values are provided for the solid lines. The color bar is the natural logarithm of the ratio of  $>51 \mu\text{m}$  PIC : BSi at  $z_{\text{PAR}}$ . We interpret all warm colors  $>0$  to indicate stations with a high relative abundance of coccolithophores, and all cool values  $<0$  to indicate stations with a high relative abundance of diatoms (Figs. S2, S3). A few station numbers discussed in the text are indicated. Refer to Fig. 1 for station locations.

#### 4.6 Mineral–POC flux correlations in the mesopelagic zone

To directly test whether minerals facilitate POC transfer through the upper mesopelagic zone of the water column as well, we compared flux transfer efficiencies 100 m below the base of the euphotic zone ( $T_{100}$ ) with BSi and PIC fluxes at  $z_{\text{PAR}}$  (Fig. 9c, d). If the mineral ballast model were to apply to the upper mesopelagic zone, one would expect greater transfer efficiencies (i.e., lower attenuation of POC flux) in regions of higher mineral export. The data highlight several key differences between the role of minerals in the euphotic and upper mesopelagic zones. For one, the correlation between PIC flux and  $T_{100}$ , excluding values at GB1-25 and GB2-106, is significantly positive ( $p < 0.001$ ,  $r^2 = 0.39$ ). The relationship remains even when assessing data from each cruise individually (for GB1,  $p = 0.047$ ,  $r^2 = 0.34$ ; for GB2,  $p = 0.009$ ,  $r^2 = 0.52$ ), lending further support to a potential role for PIC in POC transfer through the upper mesopelagic zone.

Further, there was no significant correlation, with or without GB1-25 and GB2-106  $T_{100}$  values, between BSi export fluxes in GB2 and  $T_{100}$ . However, higher particulate biogenic silica concentrations ( $>51 \mu\text{m}$  [BSi]) at  $z_{\text{PAR}}$  did correspond with greater attenuation of  $>51 \mu\text{m}$  [POC] below  $z_{\text{PAR}}$  ( $p = 0.004$ ,  $r^2 = 0.35$ ; Fig. 10a), suggesting that, in contrast to its role in the euphotic zone, BSi is associated with greater degradation in the mesopelagic zone of the water column.

#### 4.7 Other controls on POC transfer

The correlation between the attenuation of  $>51 \mu\text{m}$  [POC] and the size fractionation of POC ( $\% >51 \mu\text{m}$  [POC]) at  $z_{\text{PAR}}$  is even stronger than with  $>51 \mu\text{m}$  [BSi] ( $p < 0.001$ ,  $r^2 = 0.63$ ; Fig. 10b). GB1-85 appears to be an outlier for both relationships in Fig. 10, but especially for the relationship between  $>51 \mu\text{m}$  [POC] attenuation and  $>51 \mu\text{m}$  [BSi] (Fig. 10a). The correlation remains significant when the high [BSi] value from station GB1-85 is removed. Notably, the power-law fit at GB1-85 is not very good in the upper mesopelagic; fitting  $>51 \mu\text{m}$  [POC] between  $z_{\text{PAR}}$  and 500 m yields a better fit (higher  $r^2$ ; see Fig. 3) with a higher attenuation coefficient of 2.35 (compared to 1.7 for the entire mesopelagic zone). This modified upper mesopelagic attenuation at GB1-85 improves the overall correlations between the attenuation coefficient and both  $>51 \mu\text{m}$  [BSi] ( $p < 0.001$ ,  $r^2 = 0.60$ ) and  $\% >51 \mu\text{m}$  [POC] ( $p < 0.001$ ;  $r^2 = 0.78$ ), further strengthening the argument that  $>51 \mu\text{m}$  [BSi] and  $\% >51 \mu\text{m}$  [POC] at  $z_{\text{PAR}}$  are important factors in POC transfer in the upper mesopelagic zone.

The relationships between the attenuation of  $>51 \mu\text{m}$  [POC] and  $>51 \mu\text{m}$  [BSi] and particle size fractionation may arise from a more fundamental feature shared by both high-[BSi] and large-particle stations of the Great Calcite Belt: diatom-rich phytoplankton communities. Indeed, we also observe a strong correlation between  $>51 \mu\text{m}$  [BSi] and  $\% >51 \mu\text{m}$  [POC] at  $z_{\text{PAR}}$  ( $p < 0.001$ ,  $r^2 = 0.65$ ; not shown). This is a consistent feature across diatom-rich populations, which produce large, BSi-rich organic aggregates that sink rapidly out of the euphotic zone (Michaels and Silver, 1988; Buesseler, 1998; Thomalla et al., 2006). Indeed, euphotic zone diatom abundances enumerated with a FlowCam<sup>®</sup> are significantly correlated with  $>51 \mu\text{m}$  [BSi] at  $z_{\text{PAR}}$  at corresponding stations in GB1 and GB2 (Fig. S2a). Thus, characteristics describing ecosystem structure may underlie the correlation between BSi export and POC export in the Great Calcite Belt (Francois et al., 2002; Thomalla et al., 2008; Henson et al., 2012a, b).

However, ecosystem composition does not directly explain why larger particles exported into the mesopelagic zone are remineralized more vigorously hundreds of meters below (Fig. 10b). It is paradoxical that the same large particles that sink quickly out of the euphotic zone would then remineralize faster as well. This association between attenuation coefficient and particle size suggests that these particles sink more slowly than expected in the mesopelagic zone given their size (for example, as a result of high porosity and low excess density), and/or that they are subject to faster remineralization compared to regions with more POC in the small size fraction. Francois et al. (2002) noted a negative relationship between bathypelagic transfer efficiency and opal flux, and attributed this to increased lability in large diatom aggregates. Though we do not observe any negative correlation between upper mesopelagic transfer efficiency ( $T_{100}$ ) and BSi

fluxes at  $z_{\text{PAR}}$ , we suggest that potentially higher degradability of POC produced by diatom-rich communities may similarly explain the relationship between particle size and  $>51 \mu\text{m}$  [POC] attenuation in the upper mesopelagic zone.

The view of POC quality as a driving factor behind POC transfer argues for a deterministic role of euphotic zone community structure in POC transfer below the euphotic zone. It supports the conventional perspective that diatom-dominated communities are strong exporters of large, sinking POC particles out of the euphotic zone (Buesseler, 1998; Guidi et al., 2009), but it also adds to the growing view that these communities have poor transfer efficiency and high attenuation through the mesopelagic zone (Francois et al., 2002; Guidi et al., 2009; Henson et al., 2012a, b).

For instance, station GB1-85, with over half of the [POC] in the  $>51 \mu\text{m}$  size class fraction in the euphotic zone (Fig. 6c; Table 3), has a low  $>51 \mu\text{m}$  [PIC]:[BSi] ratio of 0.035 at  $z_{\text{PAR}}$  (indicated in log scale in Fig. 10a and b), which indicates relatively high diatom populations producing large BSi-rich aggregates (Figs. 2, S2, S3). Station GB1-85 exhibits a high export efficiency (Ez ratio = 0.38, within the upper quartile of the data set), and the highest  $>51 \mu\text{m}$  [POC] and export fluxes at  $z_{\text{PAR}}$  (Figs. 5b, 7b, 8a; Table 3). Notably,  $>51 \mu\text{m}$  [POC] values in the lower mesopelagic zone are also the highest at GB1-85, despite attenuating greatly below  $z_{\text{PAR}}$  (attenuation coefficient = 1.7; Figs. 3, 8b, c; Table 2). But, because of high attenuation, proportionally less organic carbon transfers to the deep sea at GB1-85. The same diatom-rich communities that vigorously export POC ultimately may not sequester as much organic carbon in the deep ocean or draw down as much atmospheric  $\text{CO}_2$  (Kwon et al., 2009) as would be expected considering the magnitude of export alone.

In contrast to a model diatom community like station GB1-85, station GB1-25 is BSi-depleted, with a  $>51 \mu\text{m}$  [PIC]:[BSi] ratio of 1.4 at  $z_{\text{PAR}}$  (indicated in log scale in Fig. 10a), indicating relatively more coccolithophores in the community (Figs. S2, S3). With proportionally less POC in the  $>51 \mu\text{m}$  size fraction (only 3.2%; Figs. 6c, 10b; Table 3),  $>51 \mu\text{m}$  [POC] at GB1-25 attenuates little through the mesopelagic zone (attenuation coefficient = 0.4, the lowest of the data set) such that a third of the  $>51 \mu\text{m}$  [POC] at  $z_{\text{PAR}}$  remains at 1000 m, compared to only 1.4% at station GB1-85 (Fig. 3). At GB1-25, export efficiency is very low (Ez ratio = 0.04), suggesting that the particles exiting the euphotic zone here have been recycled vigorously in the euphotic zone prior to export, which may explain their low  $>51 \mu\text{m}$  [POC] and high proportion in the  $<51 \mu\text{m}$  size fraction at  $z_{\text{PAR}}$ . In the mesopelagic zone, these particles are not very reactive and thus remineralize very little, perhaps sequestering a higher proportion of the  $\text{CO}_2$  fixed in the euphotic zone.

Several other stations with proportionally more small particles and weaker  $>51 \mu\text{m}$  [POC] attenuation in the mesopelagic zone exhibit higher  $>51 \mu\text{m}$  [PIC] than  $>51 \mu\text{m}$

[BSi] at  $z_{\text{PAR}}$  (labeled in the lower left quadrant of Fig. 10b), suggesting that export regimes characterized by high relative abundance of coccolithophores consistently transfer less reactive POC to the mesopelagic zone. Artificial roller tank experiments have demonstrated that coccolithophore cultures can produce smaller, more compact aggregates than diatom cultures, partly because of smaller cell sizes (Iversen and Ploug, 2010). However, smaller size does not necessarily mean slower sinking velocities (e.g., McDonnell and Buesseler, 2010). Iversen and Ploug (2010) showed that the higher excess density of these small aggregates generated faster sinking speeds than similarly sized pure diatom aggregates. Another roller tank study that compared aggregate formation by calcifying versus non-calcifying coccolithophores observed that aggregates formed from calcifying coccolithophores were smaller but faster sinking (Engel et al., 2009). In regions like the Great Calcite Belt, dense coccolithophore populations may similarly export small, highly degraded and compact particles out of the euphotic zone. As a result, these communities would efficiently transfer POC towards the base of the mesopelagic zone, even if the magnitude of exported POC is not as high as in diatom-rich regions (Thomalla et al., 2008; Guidi et al., 2009; Henson et al., 2012b). This may explain why higher PIC export fluxes are associated with higher transfer efficiencies but not higher POC flux at  $z_{\text{PAR}}$  (Fig. 9), and also why the ballast association between PIC and POC fluxes appears only at greater depths (Francois et al., 2002; Klaas and Archer, 2002).

Attenuation coefficients for  $>51 \mu\text{m}$  [POC] across diatom-rich regions exhibit a great spread ( $\text{SD} = 0.47$ ), ranging from 0.47 to 1.88. Not all diatom-rich stations (i.e.,  $>51 \mu\text{m}$  [PIC]:[BSi]  $< 1$  at  $z_{\text{PAR}}$ ) have proportionally larger particles or higher b-values (e.g., stations GB1-70, GB1-77 and GB2-87; Fig. 10b). In contrast, attenuation coefficients across coccolithophore-rich regions (i.e.,  $>51 \mu\text{m}$  [PIC]:[BSi]  $\geq 1$  at  $z_{\text{PAR}}$ ) exhibit a lower standard deviation (0.31) and a smaller range, 0.35 to 1.12. The greater variance in attenuation across BSi-rich regions may result from sampling the diatom populations at different seasons of the bloom cycle (Lam et al., 2011), and implies that there may be less seasonality in POC transfer to depth in coccolithophore-rich regions. Indeed, massive diatom export events with high transfer efficiency through the mesopelagic zone have been observed (Martin et al., 2011; Smetacek et al., 2012), so there are clearly conditions that can lead to efficient mesopelagic POC transfer from diatom blooms.

It is worth noting that  $>51 \mu\text{m}$  [PIC]:[BSi] ratios did increase with depth at most stations of the Great Calcite Belt, as might be expected because BSi is undersaturated in seawater. The possibility that BSi dissolves faster than PIC in particles sinking through the mesopelagic zone would complicate the connections we draw between diatom-rich communities in the euphotic zone and the attenuation of  $>51 \mu\text{m}$  [POC]. However, there are no associations between the magnitude of [PIC]:[BSi] increase and  $>51 \mu\text{m}$  [BSi] at  $z_{\text{PAR}}$ ,  $>51 \mu\text{m}$

[PIC] at  $z_{\text{PAR}}$  or  $> 51 \mu\text{m}$  [POC] attenuation with depth, suggesting that the issue of differential dissolution should not significantly impact our earlier interpretations. In the future, directly evaluating the degradability of sinking POC using organic characterization techniques (e.g., ramped pyrolysis or biomarker isolation; e.g., Wakeham et al., 2002; Rosenheim et al., 2008, 2013; Rosenheim and Galy, 2012) would greatly improve our ability to track the transformation of POC produced by different ecosystem assemblages across the Great Calcite Belt.

## 5 Conclusions

In summary, we argue here that phytoplankton assemblages play a fundamental role (Francois et al., 2002; Thomalla et al., 2008; Henson et al., 2012a, b) in determining the fate of POC export through the Great Calcite Belt region, the effect of which sometimes, but not always, appears as a mineral ballast mechanism in the euphotic zone (Lam et al., 2011; Henson et al., 2012a; Lima et al., 2014). Though shallow BSi export fluxes were strongly correlated with POC export fluxes, they are also associated with diatom communities that produce larger particles that attenuate more quickly through the mesopelagic zone, such that proportionally less POC reaches the lower mesopelagic zone, and proportionally more is returned to the water column as remineralized carbon (dissolved inorganic and organic carbon).

**The Supplement related to this article is available online at doi:10.5194/bg-12-3953-2015-supplement.**

*Author contributions.* S. Z. Rosengard, the primary author, participated in the GB2 field work, sample analysis in the lab, and writing. P. J. Lam contributed to field work during GB2, and participated in both data interpretation and editing of the manuscript. W. M. Balch, supplied the primary productivity and light profile data included here, as well as coccolithophore and diatom cell count data in the Supplement, and provided valuable feedback during writing. M. E. Auro and S. Pike participated in field work and sample analysis during and after GB1. D. Drapeau and B. Bowler contributed to field work during both GB1 and GB2, as well as sample analysis, particularly with respect to primary productivity and light profile data.

*Acknowledgements.* Many thanks to Ken Buesseler for discussions and lending us field equipment; Dan Ohnemus, Angela Warner, Michael Brown, Rebecca Fowler, and Marina Van der Eb for help at sea; and Laura Lubelczyk, Paul Henderson, and Scott Birdwhistell for analytical work/assistance. This work was funded by NSF OCE-0960880 to P. J. Lam, and NSF OCE-0961660 and NASA NNX11A072G and NNX11AL93G to W. M. Balch.

Edited by: C. Robinson

## References

- Abramson, L., Lee, C., Liu, Z. F., Wakeham, S. G., and Szlosek, J.: Exchange between suspended and sinking particles in the north-west Mediterranean as inferred from the organic composition of in situ pump and sediment trap samples, *Limnol. Oceanogr.*, 55, 725–739, 2010.
- Armstrong, R. A., Lee, C., Hedges, J. I., Honjo, S., and Wakeham, S. G.: A new, mechanistic model for organic carbon fluxes in the ocean based on the quantitative association of POC with ballast minerals, *Deep-Sea Res. Pt. II*, 49, 219–236, 2002.
- Balch, W. M., Drapeau, D., and Fritz, J.: Monsoonal forcing of calcification in the Arabian Sea, *Deep-Sea Res. Pt. II*, 47, 1301–1337, 2000.
- Balch, W. M., Drapeau, D. T., Bowler, B. C., Lyczkowski, E., Booth, E. S., and Alley, D.: The contribution of coccolithophores to the optical and inorganic carbon budgets during the Southern Ocean Gas Exchange Experiment: New evidence in support of the Great Calcite Belt hypothesis, *J. Geophys. Res.*, 116, C00F06, doi:10.1029/2011JC006941, 2011a.
- Balch, W. M., Poulton, A. J., Drapeau, D. T., Bowler, B. C., Windecker, L. A., and Booth, E. S.: Zonal and meridional patterns of phytoplankton biomass and carbon fixation in the Equatorial Pacific Ocean, between 110° W and 140° W, *Limnol. Oceanogr.*, 59, 1715–1732, 2011b.
- Balch, W. M., Drapeau, D. T., Bowler, B. C., Lyczkowski, E. R., Lubelczyk, L. C., Painter, S. C., and Poulton, A. J.: Surface biological, chemical, and optical properties of the Patagonian Shelf coccolithophore bloom, the brightest waters of the Great Calcite Belt, *Limnol. Oceanogr.*, 59, 1715–1732, 2014.
- Belkin, I. M. and Gordon, A. L.: Southern Ocean fronts from the Greenwich meridian to Tasmania, *J. Geophys. Res.-Oceans*, 101, 3675–3696, 1996.
- Bishop, J. K. B., Lam, P. J., and Wood, T. J.: Getting good particles: accurate sampling of particles by large volume in-situ filtration, *Limnol. Oceanogr.-Methods*, 10, 681–710, 2012.
- Brzezinski, M. A. and Nelson, D. M.: Seasonal changes in the silicon cycle within a Gulf Stream warm-core ring, *Deep-Sea Res. Pt. I*, 36, 1009–1030, 1989.
- Buesseler, K. O.: The decoupling of production and particulate export in the surface ocean, *Global Biogeochem. Cy.*, 12, 297–310, 1998.
- Buesseler, K. O. and Boyd, P.: Shedding light on processes that control particle export and flux attenuation in the twilight zone of the open ocean, *Limnol. Oceanogr.*, 54, 1210–1232, 2009.
- Buesseler, K. O., Ball, L., Andrews, J., Cochran, J. K., Hirschberg, D. J., Bacon, M. P., Fleer, A., and Brzezinski, M.: Upper ocean export of particulate organic carbon and biogenic silica in the Southern Ocean along 170 degrees W, *Deep-Sea Res. Pt. II*, 48, 4275–4297, 2001.
- Buesseler, K. O., Barber, R. T., Dickson, M. L., Hiscock, M. R., Moore, J. K., and Sambrotto, R.: The effect of marginal ice-edge dynamics on production and export in the Southern Ocean along 170 degrees W, *Deep-Sea Res. Pt. II*, 50, 579–603, 2003.
- Buesseler, K. O., Benitez-Nelson, C. R., Moran, S. B., Burd, A., Charette, M., Cochran, J. K., Coppola, L., Fisher, N. S., Fowler, S. W., and Gardner, W. D.: An assessment of particulate organic carbon to thorium-234 ratios in the ocean and their impact on the application of  $^{234}\text{Th}$  as a POC flux proxy, *Mar. Chem.*, 100, 213–233, 2006.

- Buesseler, K. O., Lamborg, C. H., Boyd, P. W., Lam, P. J., Trull, T. W., Bidigare, R. R., Bishop, J. K. B., Casciotti, K. L., Dehairs, F., Elskens, M., Honda, M., Karl, D. M., Siegel, D. A., Silver, M. W., Steinberg, D. K., Valdes, J., Van Mooy, B., and Wilson, S.: Revisiting carbon flux through the ocean's twilight zone, *Science*, 316, 567–570, 2007.
- Buesseler, K. O., Lamborg, C. H., Cai, P., Escoube, R., Johnson, R., Pike, S., Masque, P., McGillicuddy, D., and Verdeny, E.: Particle fluxes associated with mesoscale eddies in the Sargasso Sea, *Deep-Sea Res. Pt. II*, 55, 1426–1444, 2008.
- Buesseler, K. O., Pike, S., Maiti, K., Lamborg, C. H., Siegel, D. A., and Trull, T. W.: Thorium-234 as a tracer of spatial, temporal and vertical variability in particle flux in the North Pacific, *Deep-Sea Res. Pt. I*, 56, 1143–1167, 2009.
- Cochran, J. K., Buesseler, K. O., Bacon, M. P., Wang, H. W., Hirschberg, D. J., Ball, L., Andrews, J., Crossin, G., and Flier, A.: Short-lived thorium isotopes (Th-234, Th-228) as indicators of POC export and particle cycling in the Ross Sea, Southern Ocean, *Deep-Sea Res. Pt. II*, 47, 3451–3490, 2000.
- Coppola, L., Roy-Barman, M., Mulsow, S., Povinec, P., and Jeandel, C.: Low particulate organic carbon export in the frontal zone of the Southern Ocean (Indian sector) revealed by Th-234, *Deep-Sea Res. Pt. I*, 52, 51–68, 2005.
- De La Rocha, C. L., Nowald, N., and Passow, U.: Interactions between diatom aggregates, minerals, particulate organic carbon, and dissolved organic matter: Further implications for the ballast hypothesis, *Global Biogeochem. Cy.*, 22, doi:10.1029/2007GB003156, 2008.
- Engel, A., Szlosek, J., Abramson, L., Liu, Z., and Lee, C.: Investigating the effect of ballasting by CaCO<sub>3</sub> in *Emiliania huxleyi*: I. Formation, settling velocities and physical properties of aggregates, *Deep-Sea Res. Pt. II*, 56, 1396–1407, 2009.
- Fabry, V. J. and Balch, W. M.: Direct measurements of calcification rates in planktonic organisms, in: *Guide to Best Practices in Ocean Acidification Research and Data Reporting*, edited by: Riebeseil, U., Fabry, V. J., Hansson, L., and Gattuso, J.-P., European Project on Ocean Acidification (EPOCA), Bremerhaven, Germany, 185–196, 2010.
- Francois, R., Honjo, S., Krishfield, R., and Manganini, S.: Factors controlling the flux of organic carbon to the bathypelagic zone of the ocean, *Global Biogeochem. Cy.*, 16, 34-1–34-20, doi:10.1029/2001GB001722, 2002.
- Friedrich, J. and van der Loeff, M. M. R.: A two-tracer (Po-210-Th-234) approach to distinguish organic carbon and biogenic silica export flux in the Antarctic Circumpolar Current, *Deep-Sea Res. Pt. I*, 49, 101–120, 2002.
- Giering, S. L. C., Sanders, R., Lampitt, R. S., Anderson, T. R., Tamburini, C., Boutrif, M., Zubkov, M. V., Marsay, C. M., Henson, S. A., Saw, K., Cook, K., and Mayor, D. J.: Reconciliation of the carbon budget in the ocean's twilight zone, *Nature*, 507, 480–483, 2014.
- Glover, D. M., Jenkins, W. J., and Doney, S. C.: *Modeling methods for marine science*, Cambridge University Press, New York, 27–29, 2011.
- Guidi, L., Stemann, L., Jackson, G. A., Ibanez, F., Claustre, H., Legendre, L., Picheral, M., and Gorsky, G.: Effects of phytoplankton community on production, size and export of large aggregates: A world-ocean analysis, *Limnol. Oceanogr.*, 54, 1951–1963, 2009.
- Hedges, J. I. and Oades, J. M.: Comparative organic geochemistries of soils and marine sediments, *Org. Geochem.*, 27, 319–361, 1997.
- Henson, S. A., Sanders, R., Madsen, E., Morris, P. J., Le Moigne, F., and Quartly, G. D.: A reduced estimate of the strength of the ocean's biological carbon pump, *Geophys. Res. Lett.*, 38, L04606, doi:10.1029/2011GL046735, 2011.
- Henson, S., Lampitt, R., and Johns, D.: Variability in phytoplankton community structure in response to the North Atlantic Oscillation and implications for organic carbon flux, *Limnol. Oceanogr.*, 57, 1591–1601, 2012a.
- Henson, S. A., Sanders, R., and Madsen, E.: Global patterns in efficiency of particulate organic carbon export and transfer to the deep ocean, *Global Biogeochem. Cy.*, 26, GB1028, doi:10.1029/2011GB004099, 2012b.
- Henson, S. A., Yool, A., and Sanders, R.: Variability in efficiency of particulate organic carbon export: A model study, *Global Biogeochem. Cy.*, 29, GB004965, doi:10.1002/2014GB004965, 2015.
- Honjo, S., Francois, R., Manganini, S., Dymond, J., and Collier, R.: Particle fluxes to the interior of the Southern Ocean in the Western Pacific sector along 170 degrees W, *Deep-Sea Res. Pt. II*, 47, 3521–3548, 2000.
- Iversen, M. H. and Ploug, H.: Ballast minerals and the sinking carbon flux in the ocean: carbon-specific respiration rates and sinking velocity of marine snow aggregates, *Biogeosciences*, 7, 2613–2624, doi:10.5194/bg-7-2613-2010, 2010.
- Jacquet, S. H. M., Lam, P. J., Trull, T., and Dehairs, F.: Carbon export production in the subantarctic zone and polar front zone south of Tasmania, *Deep-Sea Res. Pt. II*, 58, 2277–2292, 2011.
- Klaas, C. and Archer, D. E.: Association of sinking organic matter with various types of mineral ballast in the deep sea: Implications for the rain ratio, *Global Biogeochem. Cy.*, 16, 1116–1129, 2002.
- Kwon, E. Y., Primeau, F., and Sarmiento, J. L.: The impact of remineralization depth on the air-sea carbon balance, *Nat. Geosci.*, 2, 630–635, 2009.
- Lam, P. J. and Bishop, J. K. B.: High biomass, low export regimes in the Southern Ocean, *Deep-Sea Res. Pt. II*, 54, 601–638, 2007.
- Lam, P. J., Doney, S. C., and Bishop, J. K. B.: The dynamic ocean biological pump: Insights from a global compilation of particulate organic carbon, CaCO<sub>3</sub>, and opal concentration profiles from the mesopelagic, *Global Biogeochem. Cy.*, 25, GB3009, doi:10.1029/2010GB003868, 2011.
- Lam, P. J., Ohnemus, D. C., and Auro, M. E.: Size-fractionated major particle composition and concentrations from the US GEO-TRACES north Atlantic zonal transect, *Deep-Sea Res. Pt. II*, 116, 303–320, 2014.
- Le Moigne, F. A. C., Sanders, R. J., Villa-Alfageme, M., Martin, A. P., Pabortsava, K., Planquette, H., Morris, P. J., and Thomalla, S. J.: On the proportion of ballast versus non-ballast associated carbon export in the surface ocean, *Geophys. Res. Lett.*, 39, L15610, doi:10.1029/2012GL052980, 2012.
- Le Moigne, F. A. C., Henson, S. A., Sanders, R. J., and Madsen, E.: Global database of surface ocean particulate organic carbon export fluxes diagnosed from the <sup>234</sup>Th technique, *Earth Syst. Sci.*, 5, 295–304, doi:10.5194/essd-5-295-2013, 2013.
- Le Moigne, F. A. C., Pabortsava, K., Marcinko, C. L. J., Martin, P., and Sanders, R. J.: Where is mineral ballast important for surface

- export of particulate organic carbon in the ocean?, *Geophys. Res. Lett.*, 41, doi:10.1002/2014GL061678, GL061678, 2014.
- Lima, I. D., Lam, P. J., and Doney, S. C.: Dynamics of particulate organic carbon flux in a global ocean model, *Biogeosciences*, 11, 1177–1198, doi:10.5194/bg-11-1177-2014, 2014.
- Lomas, M. W., Steinberg, D. K., Dickey, T., Carlson, C. A., Nelson, N. B., Condon, R. H., and Bates, N. R.: Increased ocean carbon export in the Sargasso Sea linked to climate variability is countered by its enhanced mesopelagic attenuation, *Biogeosciences*, 7, 57–70, doi:10.5194/bg-7-57-2010, 2010.
- Maiti, K., Benitez-Nelson, C. R., Rii, Y., and Bidigare, R.: The influence of a mature cyclonic eddy on particle export in the lee of Hawaii, *Deep-Sea Res. Pt. II*, 55, 1445–1560, 2012.
- Martin, J. H., Knauer, G. A., Karl, D. M., and Broenkow, W. W.: Vertex – Carbon Cycling in the Northeast Pacific, *Deep-Sea Res. Pt. I*, 34, 267–285, 1987.
- Martin, P., Lampitt, R. S., Jane Perry, M., Sanders, R., Lee, C., and D'Asaro, E.: Export and mesopelagic particle flux during a North Atlantic spring diatom bloom, *Deep-Sea Res. Pt. I*, 58, 338–349, 2011.
- McCave, I. N.: Vertical flux of particles in the ocean, *Deep-Sea Res.*, 22, 491–502, 1975.
- McDonnell, A. M. P. and Buesseler, K. O.: Variability in the average sinking velocities of marine particles, *Limnol. Oceanogr.*, 55, 2085–2096, 2010.
- Michaels, A. F. and Silver, M. W.: Primary production, sinking fluxes and the microbial food web, *Deep-Sea Res. Pt. I*, 35, 473–490, 1988.
- Morris, P. J., Sanders, R., Turnewitsch, R., and Thomalla, S.: Th-234-derived particulate organic carbon export from an island-induced phytoplankton bloom in the Southern Ocean, *Deep-Sea Res. Pt. II*, 54, 2208–2232, 2007.
- Owens, S., Buesseler, K., and Sims, K.: Re-evaluating the  $^{238}\text{U}$ -salinity relationship in seawater: Implications for the  $^{238}\text{U}$ – $^{234}\text{Th}$  disequilibrium method, *Mar. Chem.*, 127, 31–39, 2011.
- Paasche, E. and Brubak, S.: Enhanced calcification in the coccolithophorid *Emiliania huxleyi* (Haptophyceae) under phosphorus limitation, *Phycologia*, 33, 324–330, 1994.
- Passow, U. and De la Rocha, C. L.: Accumulation of mineral ballast on organic aggregates, *Global Biogeochem. Cy.*, 20, doi:10.1029/2005GB002579, 2006.
- Pike, S. M., Buesseler, K. O., Andrews, J., and Savoye, N.: Quantification of Th-234 recovery in small volume sea water samples by inductively coupled plasma-mass spectrometry, *J. Radioanal. Nucl. Ch.*, 263, 355–360, 2005.
- Pilson, M. E. Q.: *An Introduction to the Chemistry of the Sea*, Cambridge University Press, New York, , 2012.
- Planchon, F., Cavagna, A.-J., Cardinal, D., André, L., and Dehairs, F.: Late summer particulate organic carbon export and twilight zone remineralisation in the Atlantic sector of the Southern Ocean, *Biogeosciences*, 10, 803–820, doi:10.5194/bg-10-803-2013, 2013.
- Resplandy, L., Martin, A. P., Le Moigne, F., Martin, P., Aquilina, A., Mémerly, L., Lévy, M., and Sanders, R.: How does dynamical spatial variability impact  $^{234}\text{Th}$ -derived estimates of organic export?, *Deep-Sea Res. Pt. I*, 68, 24–45, 2012.
- Riley, J. S., Sanders, R., Marsay, C., Le Moigne, F. A. C., Achterberg, E. P., and Poulton, A. J.: The relative contribution of fast and slow sinking particles to ocean carbon export, *Global Biogeochem. Cy.*, 26, GB1026, doi:10.1029/2011GB004085, 2012.
- Rodriguez y Baena, A. M., Boudjenoun, R., Fowler, S. W., Miquel, J. C., Masqué, P., Sanchez-Cabeza, J.-A., and Warnau, M.:  $^{234}\text{Th}$ -based carbon export during an ice-edge bloom: Sea-ice algae as a likely bias in data interpretation, *Earth Planet. Sci. Lett.*, 269, 596–604, 2008.
- Rosenheim, B. E. and Galy, V.: Direct measurement of riverine particulate organic carbon age structure, *Geophys. Res. Lett.*, 39, doi:10.1029/2012GL052883, 2012.
- Rosenheim, B. E., Day, M. B., Domack, E., Schrum, H., Ben-thien, A., and Hayes, J. M.: Antarctic sediment chronology by programmed-temperature pyrolysis: Methodology and data treatment, *Geochim. Geophys. Geosys.*, 9, doi:10.1029/2007GC001816, 2008.
- Rosenheim, B. E., Roe, K. M., Roberts, B. J., Kolker, A. S., Allison, M. A., and Johannesson, K. H.: River discharge influences on particulate organic carbon age structure in the Mississippi/Atchafalaya River System, *Global Biogeochem. Cy.*, 27, 154–166, 2013.
- Rutgers Van Der Loeff, M. M., Friedrich, J., and Bathmann, U. V.: Carbon export during the Spring Bloom at the Antarctic Polar Front, determined with the natural tracer  $^{234}\text{Th}$ , *Deep-Sea Res. Pt. II*, 44, 457–478, 1997.
- Rutgers van der Loeff, M. M., Sarin, M. M., Baskaran, M., Benitez-Nelson, C., Buesseler, K. O., Charette, M., Dai, M., Gustafsson, r., Masque, P., Morris, P. J., Orlandini, K., Rodriguez y Baena, A., Savoye, N., Schmidt, S., Turnewitsch, R., V., I., and Waples, J. T.: A review of present techniques and methodological advances in analyzing  $^{234}\text{Th}$  in aquatic systems, *Mar. Chem.*, 100, 190–212, 2006.
- Rutgers van der Loeff, M. M., Cai, P. H., Stimac, I., Bracher, A., Middag, R., Klunder, M. B., and van Heuven, S. M.:  $^{234}\text{Th}$  in surface waters: Distribution of particle export flux across the Antarctic Circumpolar Current and in the Weddell Sea during the GEOTRACES expedition ZERO and DRAKE, *Deep-Sea Res. Pt. II*, 58, 2749–2766, 2011.
- Sanders, R., Morris, P. J., Poulton, A. J., Stinchcombe, M. C., Charalampopoulou, A., Lucas, M. I., and Thomalla, S. J.: Does a ballast effect occur in the surface ocean?, *Geophys. Res. Lett.*, 37, L08602, doi:10.1029/2010GL042574, 2010.
- Santschi, P., Murray, J. W., Baskaran, M., Benitez-Nelson, C. R., Guo, L., Hung, C.-C., Lamborg, C., Moran, S. B., Passow, U., and Roy-Barman, M.: Thorium speciation in seawater, *Mar. Chem.*, 100, 250–268, 2006.
- Sarmiento, J. L., Dunne, J., Gnanadesikan, A., Key, R. M., Matsumoto, K., and Slater, R.: A new estimate of the  $\text{CaCO}_3$  to organic carbon export ratio, *Global Biogeochem. Cy.*, 16, 54-1–54-12, 2002.
- Sarmiento, J. L., Gruber, N., Brzezinski, M. A., and Dunne, J. P.: High-latitude controls of thermocline nutrients and low latitude biological productivity, *Nature*, 427, 56–60, 2004.
- Savoye, N., Benitez-Nelson, C., Burd, A. B., Cochran, J. K., Charette, M., Buesseler, K. O., Jackson, G. A., Roy-Barman, M., Schmidt, S., and Elskens, M.: Th-234 sorption and export models in the water column: A review, *Mar. Chem.*, 100, 234–249, 2006.

- Savoye, N., Trull, T. W., Jacquet, S. H. M., Navez, J., and Dehairs, F.:  $^{234}\text{Th}$ -based export fluxes during a natural iron fertilization experiment in the Southern Ocean (KEOPS), *Deep-Sea Res. Pt. II*, 55, 841–855, 2008.
- Shimmiel, G. B., Ritchie, G. D., and Fileman, T. W.: The Impact of Marginal Ice-Zone Processes on the Distribution of Pb-210, Po-210 and Th-234 and Implications for New Production in the Bellingshausen Sea, Antarctica, *Deep-Sea Res. Pt. II*, 42, 1313–1335, 1995.
- Smetacek, V., Klaas, C., Strass, V. H., Assmy, P., Montresor, M., Cisewski, B., Savoye, N., Webb, A., d'Odivio, F., Arrieta, J. M., Bathmann, U., Bellerby, R., Berg, G. M., Croot, P., Gonzalez, S., Henjes, J., Herndl, G. J., Hoffmann, L. J., Leach, H., Losch, M., Mills, M. M., Neill, C., Peeken, I., Röttgers, R., Sachs, O., Sauter, E., Schmidt, M. M., Schwarz, J., Terbrüggen, A., and Wolf-Gladrow, D.: Deep carbon export from a Southern Ocean iron-fertilized diatom bloom, *Nature*, 487, 313–319, 2012.
- Sokolov, S. and Rintoul, S. R.: Circumpolar structure and distribution of the Antarctic Circumpolar Current fronts: 1. Mean circumpolar paths, *J. Geophys. Res.-Oceans*, 114, doi:10.1029/2008JC005108, 2009.
- Steinberg, D. K., Van Mooy, B. A. S., Buesseler, K. O., Boyd, P. W., Kobari, T., and Karl, D. M.: Bacterial vs. zooplankton control of sinking particle flux in the ocean's twilight zone, *Limnol. Oceanogr.*, 53, 1327–1338, 2008.
- Strickland, J. D. and Parsons, T. R.: A practical handbook of seawater analysis, Fisheries Research Board of Canada Ottawa, 1968.
- Thomalla, S., Turnewitsch, R., Lucas, M., and Poulton, A.: Particulate organic carbon export from the North and South Atlantic gyres: The  $^{234}\text{Th}/^{238}\text{U}$  disequilibrium approach, *Deep-Sea Res. Pt. II*, 53, 1629–1648, 2006.
- Thomalla, S. J., Poulton, A. J., Sanders, R., Turnewitsch, R., Holligan, P. M., and Lucas, M. I.: Variable export fluxes and efficiencies for calcite, opal, and organic carbon in the Atlantic Ocean: A ballast effect in action?, *Global Biogeochem. Cy.*, 22, GB1010, doi:10.1029/2007GB002982, 2008.
- Trull, T. W., Bray, S. G., Buesseler, K. O., Lamborg, C. H., Mangani, S., Moy, C., and Valdes, J.: In situ measurement of mesopelagic particle sinking rates and the control of carbon transfer to the ocean interior during the Vertical Flux in the Global Ocean (VERTIGO) voyages in the North Pacific, *Deep-Sea Res. Pt. II*, 55, 1684–1695, 2008.
- Volk, T. and Hoffert, M. I.: Ocean carbon pumps: Analysis of relative strengths and efficiencies in ocean-driven atmospheric  $\text{CO}_2$  changes, *Geophysical Monographs*, 32, 99–110, 1985.
- Wakeham, S. G., Peterson, M. L., Hedges, J. I., and Lee, C.: Lipid biomarker fluxes in the Arabian Sea, with a comparison to the equatorial Pacific Ocean, *Deep-Sea Res. Pt. II*, 49, 2265–2301, 2002.
- Wilson, J. D., Barker, S., and Ridgwell, A.: Assessment of the spatial variability in particulate organic matter and mineral sinking fluxes in the ocean interior: Implications for the ballast hypothesis, *Global Biogeochem. Cy.*, 26, GB4011, doi:10.1029/2012GB004398, 2012.
- Wilson, S. E., Steinberg, D. K., and Buesseler, K. O.: Changes in fecal pellet characteristics with depth as indicators of zooplankton repackaging of particles in the mesopelagic zone of the subtropical and subarctic North Pacific Ocean, *Deep-Sea Res. Pt. II*, 55, 1636–1647, 2008.
- Zhou, K., Nodder, S. D., Dai, M., and Hall, J. A.: Insignificant enhancement of export flux in the highly productive subtropical front, east of New Zealand: a high resolution study of particle export fluxes based on  $^{234}\text{Th}$ – $^{238}\text{U}$  disequilibria, *Biogeosciences*, 9, 973–992, doi:10.5194/bg-9-973-2012, 2012.